Chapter 3

WOCE observations of the Leeuwin Current System at 22°S

3.1 INTRODUCTION

In this chapter, the ICM6 observations are used to investigate the near 2–year mean, seasonal cycle and interannual variability of the Leeuwin Current System at 22°S. The observations comprise direct current measurements and hydrographic and upper ocean current fields obtained during cruise surveys across the array. Complementary data are used to assist the interpretation of the ICM6 observations in a regional context.

3.2 DATA DESCRIPTION

3.2.1 ICM6

As part of the Australian contribution to the World Ocean Circulation (WOCE) programme, the ICM6 experiment [**Figure 3.1**] gathered *in situ* observations of the Leeuwin Current System at 22°S from moored instruments and five hydrographic surveys between August 1994 and June 1996. Principal investigators were Matthias Tomczak (Flinders University), Susan Wijffels and John Church (CSIRO Marine Research). For this study, the current meter data were directly provided by the principal investigators and processed following WOCE requirements as detailed in Domingues *et al.* [1999a]. The final product and technical reports are now part of the WOCE Global Data v3.0 [WDPC/WIPO, 2002]. The Conductivity–Temperature–Depth (CTD) data were obtained from the CSIRO Marine Data Centre [*http://www.marine.csiro.au/datacentre/*] for the R/V Franklin voyages and from the WOCE Global Data v2.0 [WDPC/WIPO, 2000] for the R/V Knorr voyage. Shipboard Acoustic Doppler Current Profiler (SADCP) data, in the same version as prepared for the WOCE Global Data v3.0, were retrieved from an online inventory at the Joint Archive for SADCP [*ftp://ilikai.soest.hawaii.edu/caldwell_pub/adcp/INVNTORY/wocetot.html*].

3.2.1.1 Moored observations

Six current meter moorings along a line extending 150 km offshore from North West Cape, near 22°S, were deployed during late August 1994, on a ridge surrounded by two canyons at the point where the wide NW shelf suddenly narrows, before widening again, in water depths between 250 and 3050 m [**Figure 3.1**]. The current meter array consisted of four RD Instruments upward–looking Acoustic Doppler Current Profilers (ADCPs), five Neil Brown Acoustic Current Meters (ACM2s) and thirteen Aanderaa recording current meters (RCMs) as shown in **Figure 3.2**. All moorings were recovered during early June 1996, except for moorings 4 and 5, for which the acoustic releases failed. The upper two instruments on mooring 5 and the deepest instrument on mooring 4 were subsequently retrieved by trawling, though the upper four instruments on mooring 4 were lost altogether. The three remaining instruments on mooring 5 were later recovered by trawling during a subsequent cruise in August/September 1996.

Despite recovery of eighteen of the twenty two current meters, data quality for speed, direction and temperature fell short of expectations while pressure records were deemed suspicious altogether [Domingues *et al.*, 1999a]. Timelines in **Table 3.1** summarise the data return for the individual current meters. The near total instrument loss on mooring 4 caused the partition of the array into two sections:

- Moorings 1, 2 and 3 refer to the inshore section, in which observations approximately spanned depths from 50 to 250 m for the entire period (September 1994 – May 1996), or from 50 to 490 m for a shorter time period (until November/ December 1995).

- Moorings 5 and 6 refer to the offshore section. Observations on mooring 5 spanned depths between 515 and 1515 m from September 1994 to November/December 1995. Observations on mooring 6 spanned depths between 785 and 2541 m, in addition to only temperature at 285 m, for the entire period (September 1994 – May 1996).

After quality control, the current meter observations were subjected to gap filling, low pass filtering and decimation. Data gaps of up to 3h, up to 24 h and up to 12 days were respectively filled using a linear interpolation, a cubic spline interpolation and a spectral interpolation [Smylie *et al.*, 1973; Ulrich *et al.*, 1973; Andersen, 1974]. The low pass filter applied was a cosine Lanczos (Lancz–6) with a cutoff period of 40 h, designed to suppress inertial (32h at 22°S), tidal and other higher frequency fluctuations. The energy response of the filter is 25% at 40 h (0.6 cpd) and 0.01% at 32 h (0.744 cpd). The current and temperature observations were decimated to six–hourly sampling, with values at 0300, 0900, 1500 and 2100 UTC.

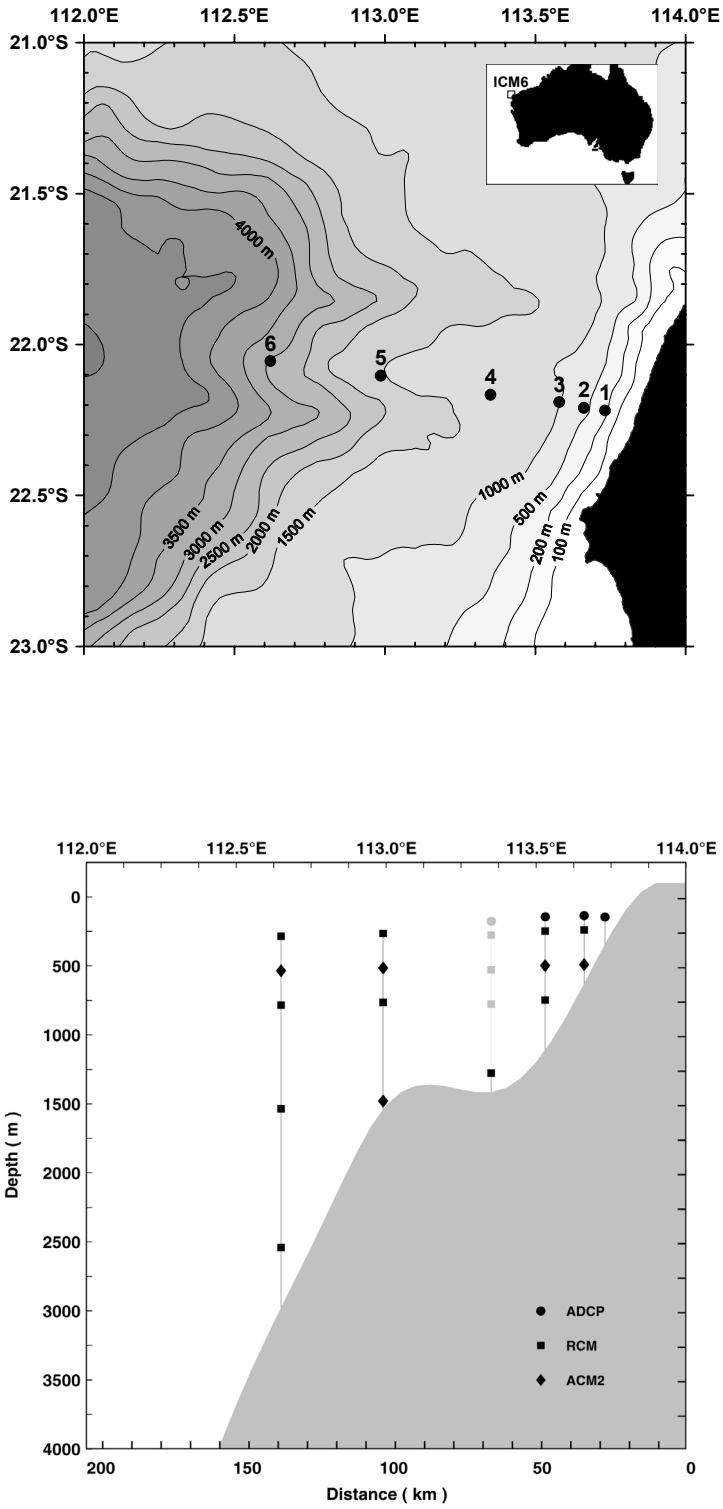

Figure 3.1. ICM6 array location (top) and current meter distribution (bottom). Gray symbols denote instruments that were not recovered on mooring 4.

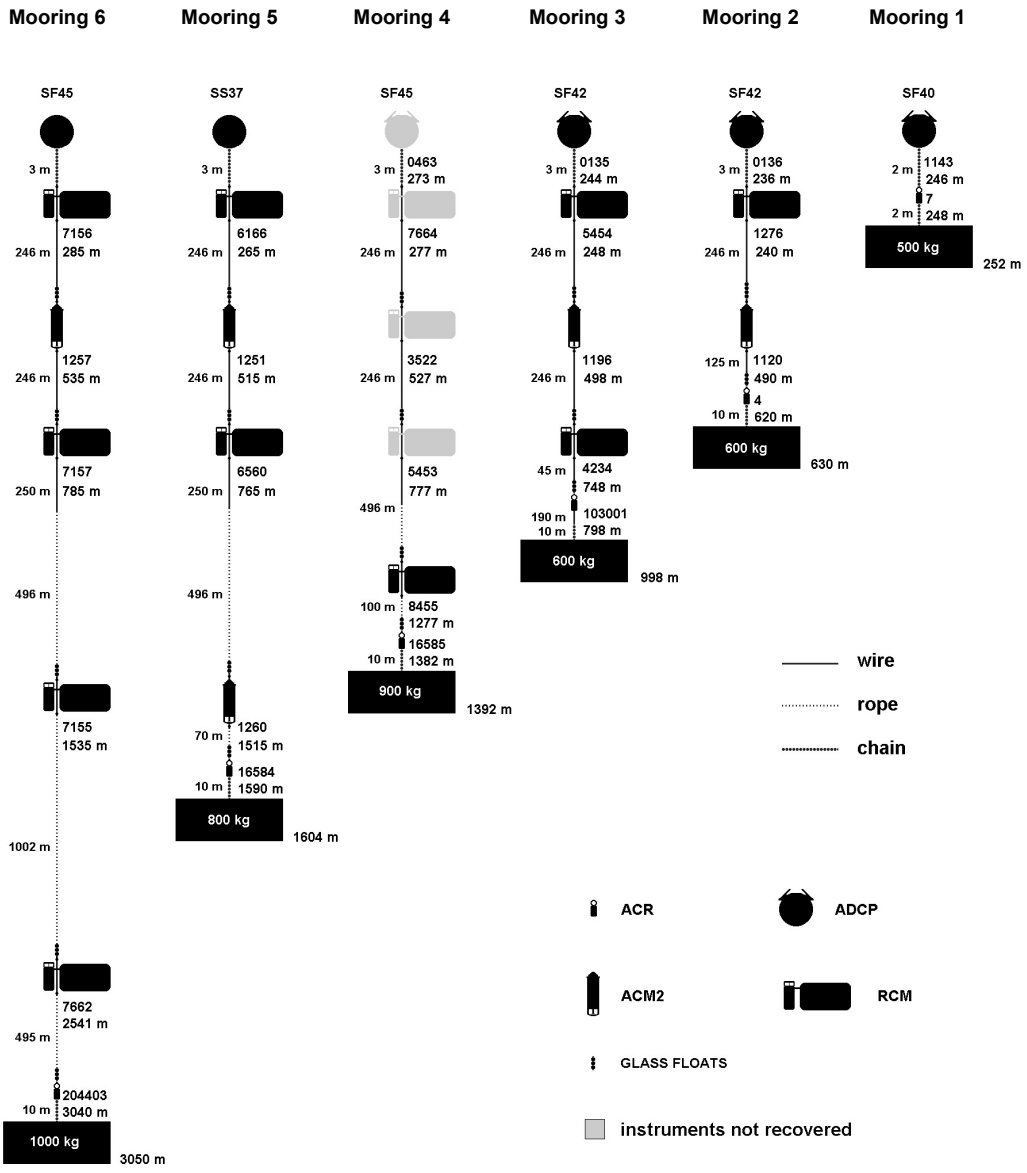

Figure 3.2. ICM6 array configuration. Identification numbers and depth positions are respectively on the right and below each instrument. Water depths are given at the base of each mooring line. ACR (acoustic release). SF and SS (surface floats). ADCP (acoustic current Doppler profiler). RCM (mechanical recording current meter). ACM2 (acoustic current meter).

Table 3.1. ICM6 data return time series. Speed gaps are indicated in days.

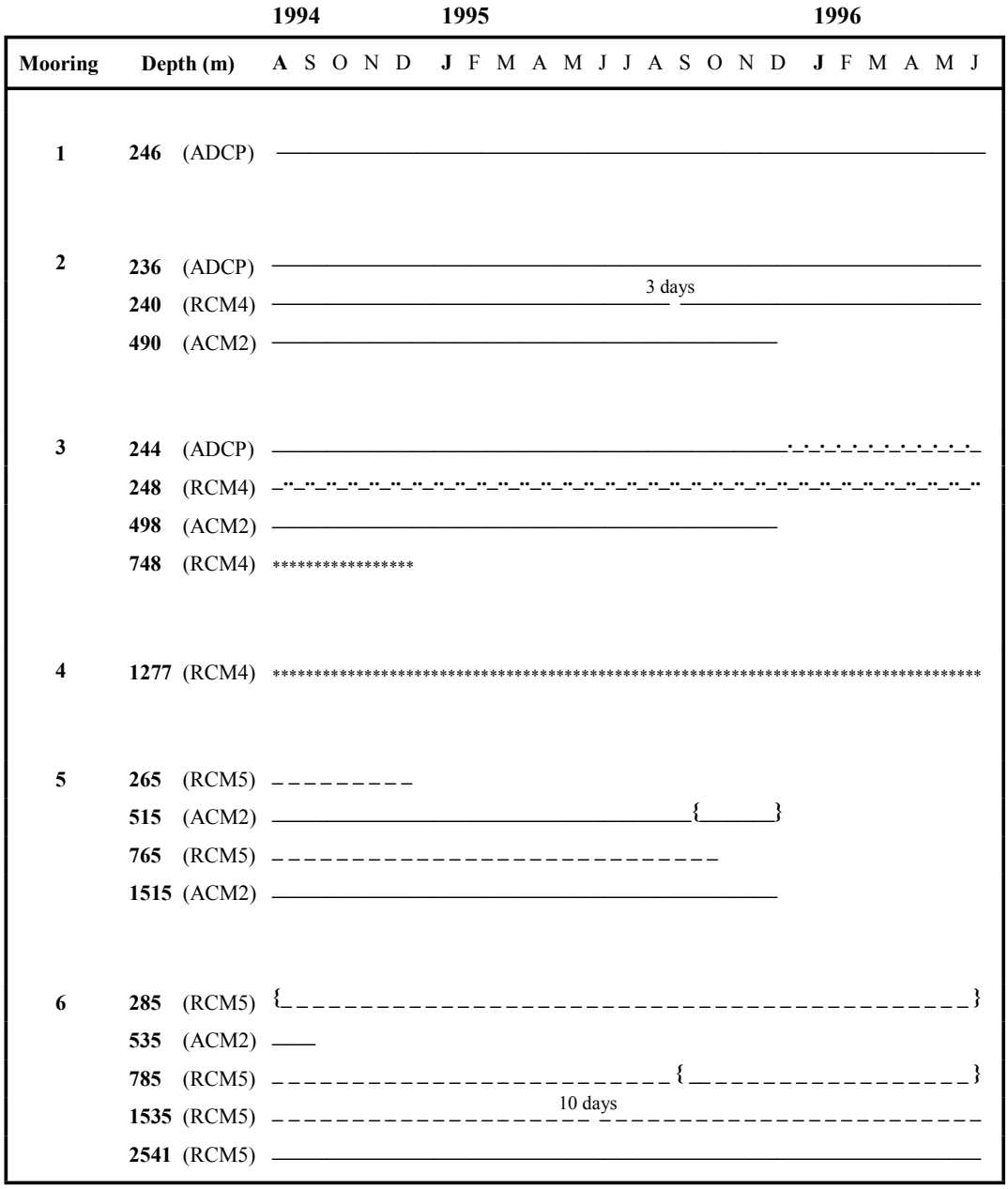

———	useful speed, direction and temperature data
{_____}	useful direction and temperature data; no useful speed data
– – – – –	useful speed, direction, temperature and pressure data
{_ _ _ _}	useful direction, temperature and pressure data; no useful speed data
–··–··–··	useful speed, direction data; good temperature variation but incorrect trend and values
–·–·–·–·	additional synthetic temperature data
*******	no useful data

3.2.1.2 Synoptic observations

The CTD and the underway SADCP observations were measured during a total of five surveys across the ICM6 array [**Table 3.2**], comprising the deployment (FR 08/94) and recovery (FR 06/96) cruises and three other voyages (FR 03/95, KN 145/8 and FR 05/96). As same year occupations occurred in a short time interval – FR 03/95 and KN 145/8 in 1995, and FR 05/96 and FR 06/96 in 1996 – there are only three distinct periods to consider: August 1994, April 1995, and May/June 1996. The CTD data were used to examine water properties and to estimate geostrophic current shears. Stations were primarily occupied on both sides of the mooring lines, except during the deployment voyage FR 08/94 which had many stations at the mooring lines. The SADCP data from the joint archive inventory, linearly interpolated in the vertical (10 m) and hourly averaged, were used to document the upper ocean current fields, typically varying from 25 to 300 m depth. One CTD/SADCP transect across the array was completed per survey, except during FR 06/96 in which two CTD and four SADCP transects were completed [**Figure 3.3**].

3.2.2 Complementary observations

3.2.2.1 CSIRO Atlas of Regional Seas

The CSIRO Atlas of Regional Seas (CARS) is based on historical hydrographic observations from the National Oceanographic Data Centre World Ocean Database [Conkright *et al.*, 1998], CSIRO Marine Research and New Zealand Institute of Water and Atmospheric Research between 10°N and 50°S and 100°E to 180°E. The temperature and salinity maps are on a ½° horizontal resolution at 56 standard depth levels. They were produced using a four dimensional weighted least squares quadratic smoother [Dunn and Ridgway, 2002; Ridgway *et al.*, 2002].

3.2.2.2 Altimetry

The 10–day gridded maps of sea level anomaly (SLA), produced by merging altimetry observations from TOPEX/Poseidon (T/P) and ERS–1,–2 satellite missions using a global suboptimal space–time objective analysis [LeTraon *et al.*, 1998], are available on a ¼° horizontal resolution and date back to 22 October 1992. From 16 December 1993 to 31 March 1995, the maps were exclusively obtained from T/P data. SLAs over shallow waters (<1000 m depth) were discarded due to potential aliasing by tides. Also note that the closest altimetric groundtrack measurements are located just offshore mooring 6 [**Figure 3.1**], so inshore of that mooring, sea level anomalies are an extrapolation created by the mapping analysis.

Table 3.2. ICM6 cruise surveys.

Cruise	Cruise Period across ICM6					Vessel	Country
FR 08/94[1]	26	August	–	27	August	1994	Franklin	Australia
FR 03/95	21	April	–	22	April	1995	Franklin	Australia
KN 145/8	26	April	–	27	April	1995	Knorr	USA
FR 05/96	27	May	–	28	May	1996	Franklin	Australia
FR 06/96[2] leg1	2	June	–	3	June	1996	Franklin	Australia
FR 06/96[2] leg2	4	June	–	5	June	1996	Franklin	Australia

[1] Deployment cruise
[2] Recovery cruise

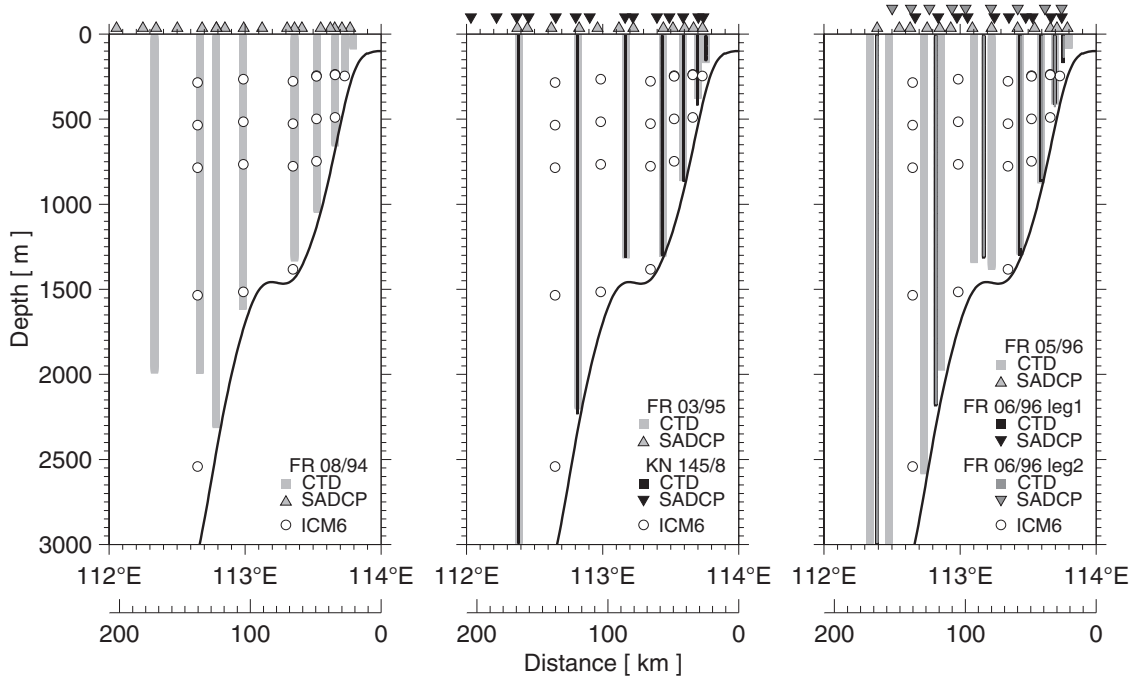

Figure 3.3. ICM6 CTD and underway SADCP sampling.

3.2.2.3 JADE and WOCE hydrographic lines

As part of the Java–Australia Dynamic Experiment (JADE) and the WOCE programme, repeat hydrographic measurements were collected across transects in the southeast Indian Ocean. The CTD data used in this study comprise two JADE transects between Port Hedland (Australia) and Bali (Indonesia), one in August 1989 (southeast monsoon, La Niña year) and another in February/March 1992 (northwest monsoon, El Niño year), and two WOCE IR6 transects from Western Australia (25°S) to Sunda Strait (Indonesia), one in April 1995 and another in September/October 1995. The JADE surveys were documented in Fieux *et al.* [1994; 1996] and Fieux and Molcard [1996] while the WOCE surveys in Sprintall *et al.* [2002] and Wijffels *et al.* [2002].

3.2.2.4 Sea Surface Temperature imagery

Sea surface temperature (SST) images were processed and provided by Chris Rathbone, Ian Barton and Paul Tildesley (CSIRO Marine Research, Hobart), with a spatial resolution of 2.2 km off Western Australia (20°–34°S, 108°–116°E). Selected images for this study refer to the periods of the ICM6 cruise surveys [**Table 3.2**].

3.2.2.5 Southern Oscillation Index

The (Troup) Southern Oscillation Index (SOI) based on the standardised anomaly of the mean sea level pressure difference between Tahiti and Darwin (Australia) was obtained from the CSIRO Atmospheric Research [*http://www.dar.csiro.au/information/soi.html*]. The index is a measure for monitoring the El Niño–Southern Oscillation (ENSO). Sustained positive (negative) values of SOI often indicate El Niño (La Niña) episodes, and the monthly index scale ranges from about –35 to +35.

3.3 RESULTS

3.3.1 Direct current observations

The cross–shelf structure of the mean currents observed during the ICM6 1994/96 experiment at 22°S is summarised in **Figure 3.4**. It shows a set of near surface currents next to the shelf break/upper slope on moorings 1, 2 and 3, and another set of deeper currents on moorings 5 and 6. The data gaps in the mooring array along with the disjointed nature of the currents, in time and space, prevented us from constructing a "full section". Alternatively we have constructed cross–shelf sections for the mean

[**Figure 3.5**] and standard deviation (std) [**Figure 3.6**] in the upper ocean near the coast, and Progressive Vector Diagrams (PVDs) to depict the displacement of the currents [**Figure 3.7**]. The cross–shelf velocity fields were not rotated into principal angles of variance since the small rotation did not change the results. The different coverage periods (363–, 463– and 640–day) in the cross–shelf sections reflect the duration of various current meter time series. The initial 363 days [panel a] is the benchmark for current comparison in the entire array [statistics in **Table 3.3**]. The 463–day mean [panel b] comprises the longest common velocity time series for the instruments that form the nearshore part of the array, moorings 1, 2 and 3. The 640–day mean [panel c], although includes fewer instruments, designates the duration of the experiment. The well known flows recognised across the ICM6 array are the poleward Leeuwin Current and the equatorward Leeuwin Undercurrent. The remaining mean currents are being documented for the first time.

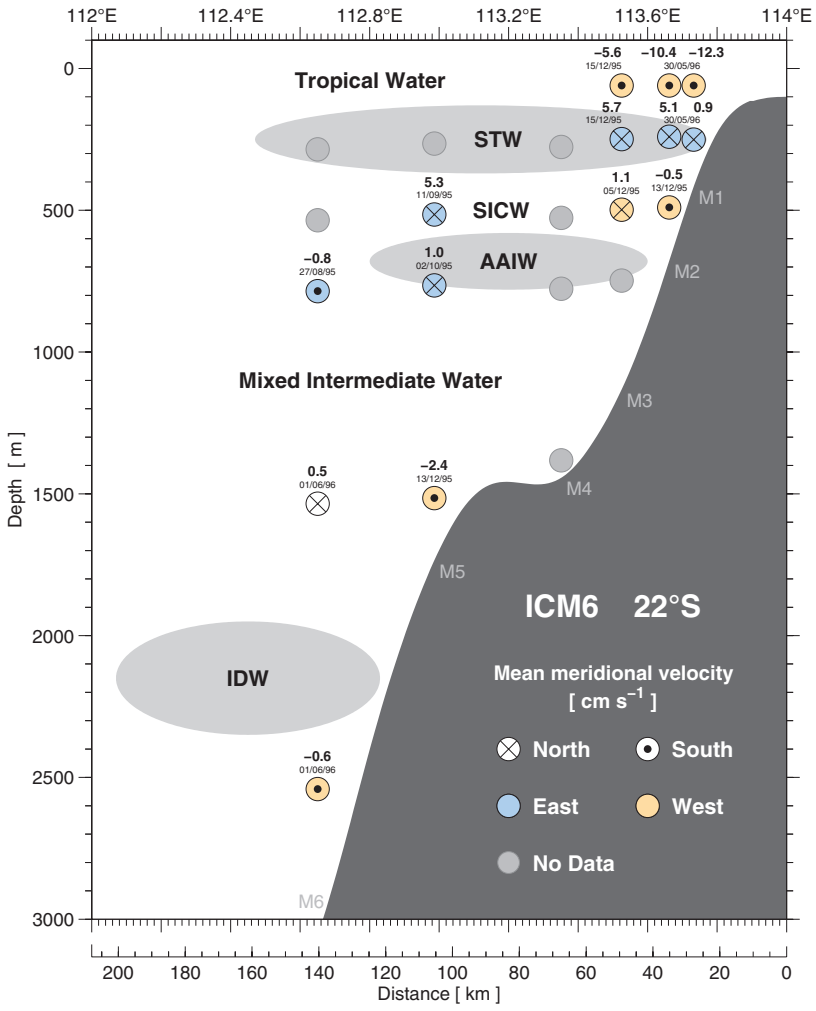

Figure 3.4. ICM6 mean current structure and water masses schematic. STW (Subtropical Water). SICW (South Indian Central Water). AAIW (Antarctic Intermediate Water). IDW (Indian Deep Water). M (mooring). The mean meridional current values were averaged from 30/08/94 to the date indicated on the top of each instrument.

3.3.1.1 Structure of the mean currents

The Leeuwin Current in the mean velocity sections [**Figure 3.5**] emerges as a coastally trapped and shallow southwestward–flowing jet that penetrates to depths of 210 m (nearshore, mooring 1) to 150 m (offshore, mooring 3). Its poleward maximum is at the shelf break (~80 m depth) but it likely extends on to the shelf. Mean maximum poleward velocities range from –6, –8 and –12 cm s^{-1} in the 363–, 463–, and 640–day averages respectively. The mean current direction is strongly aligned with the underlying continental shelf break orientation, as shown by selected ADCP bins in the PVDs [**Figure 3.7**, panel a, ~50–80 m]. Both meridional and zonal velocity fields display large fluctuations [**Figure 3.6**]. Fluctuations of the zonal velocity, despite a weak mean of –1 cm s^{-1}, might be relevant for cross–shelf exchange processes. The location of the maximum mean current is subsurface and near the coast while the standard deviation maximum is surface–intensified and slightly seaward. This organisation appears to be common in western boundary systems [e.g., Wijffels *et al.*, 1995].

Comparison of the ICM6 direct observations at 22°S with those measured during the Leeuwin Current Interdisciplinary Experiment (LUCIE) at 29.5°S [Smith *et al.*, 1991] implies that the Leeuwin Current deepens and accelerates downstream, following earlier inferences [Thompson, 1984; Godfrey and Ridgway, 1985]. LUCIE's 325–day (September 1986 to August 1987) mean velocity structure consists of a poleward flow in the top 200–250 m, with a subsurface maximum of –25 to –30 cm s^{-1} at ~80 m depth over the shelf break. So, Smith *et al.* portray a Leeuwin Current jet that is a great deal faster, at least double the magnitude, and also deeper by about 100 m from what we observe at 22°S. We suspect, however, that the Leeuwin Current might not be as slow at 22°S as the ICM6 observations indicate. Careful examination of SST imagery (not shown) during the ICM6 period reveals that the current axis often meanders back and forth across the array site [see example in **Figure 3.14**]. This underlines that the axis of the Leeuwin Current may extend well beyond mooring 3 (~113.5°E) but it also implies that the current meters on moorings 1, 2 and 3 registered "smeared" fields (smaller pointwise velocities). Although the Leeuwin Current generally meanders along its entire path, a stronger meandering behaviour is probably encouraged at North West Cape (22°S) in function of the abrupt change in the orientation of the coastline. This location is in fact a preferred site for the eddy detachment and the offshore radiation of Rossby waves [Potemra, 2001; Fang and Morrow, 2003].

The Leeuwin Undercurrent is found slightly to the west and below the Leeuwin Current [**Figure 3.5**], with an equatorward mean maximum velocity of 4 to 6 cm s^{-1} at ~210 m depth (mooring 3). We suspect the true current maximum is potentially faster and further seaward though. Topography steering appears as a major controlling factor near the upper slope, on moorings 1, 2 and 3 [**Figure 3.7**, panel a, ~210 m]. It is not clear how far the undercurrent extends beyond mooring 5 (~113°E). In terms of depth, it certainly reaches to 515 m, and less confidently, to 765 m. The net northeast flow in the

PVD from mooring 5 at 515 m [**Figure 3.7**, panel c] is persistent and the same does not seem valid for the PVD at 765 m [panel d], suggesting that the deepest level of the undercurrent must lie around those depths.

In the 325–day LUCIE experiment, from September 1986 to August 1987, Smith *et al.* [1991] report a mean maximum equatorward velocity of 9.2 cm s^{-1} at 450 m depth for a similarly marginally resolved Leeuwin Undercurrent. The depth variation of the "maximum", from ~200 m at 22°S to 450 m at 29.5°S, seems an expected response to the poleward deepening of the Leeuwin Current, but would the latitudinal difference in magnitude be an evidence for the undercurrent's weakening along its path ? Some studies generally agree that the Leeuwin Undercurrent rises and weakens as it moves equatorward [Thompson, 1984; Weaver and Middleton, 1989; Batteen and Rutherford, 1990].

A narrow mean poleward flow, flanked by the continental slope and the Leeuwin Undercurrent, is disclosed in the cross–shelf section at 490 m depth [**Figure 3.5**, panels a1 and b1]. Its poleward maximum is about –2.6 cm s^{-1} in the 363–day mean but it vanishes to –0.5 cm s^{-1} in the 463–day mean due to a current reversal as depicted in **Figure 3.7** [panel b, 490 m]. What caused this reversal is not obvious, however, if current meters are placed near the boundaries of distinct regimes, any small long term weaving of the water column may result in sampling of unlike currents by the same instrument. The question arising after the observation of this narrow poleward flow is whether it represents a deeper extension of the Leeuwin Current or an isolated bottom–trapped current.

A bottom–intensified mean poleward current of –2.4 cm s^{-1} is observed at 1515 m on mooring 5 but not at 1535 m, in a not so far distant mooring 6, where the flow instead oscillates in the north–south direction [**Figure 3.7**, panel e]. Net poleward currents at 785 m [panel d] and 2541 m [panel f] occur above and below the 0.5 cm s^{-1} net equatorward flow at 1535 m on mooring 6. Despite a net northwestward motion during the initial 363 days, the current at 2541 m depicts a persistent southwest displacement for the remaining 277 days. The mean southeast flow at 785 m and the mean southwest flow at 2541 m are in the order of –0.8 cm s^{-1} and –0.6 cm s^{-1} respectively.

Reid [2003] provides maps of large scale geostrophic flow patterns in the Indian Ocean at various depth levels, constructed in major part with observations from the WOCE Indian hydrographic program. A poleward flow along the west Australian coast is inferred from 10° to 32°S, and in depth from 200 to 3500 db. The major discrepancy of these maps with the ICM6 direct observations at 22°S is the lack of an equatorward Leeuwin Undercurrent, at least between 200–500 m depth. Although the WOCE observations were complemented with data from other programs in the Indian Ocean, we suspect that Reid's maps still do not contain sufficient information to represent the mean boundary flows off Western Australia.

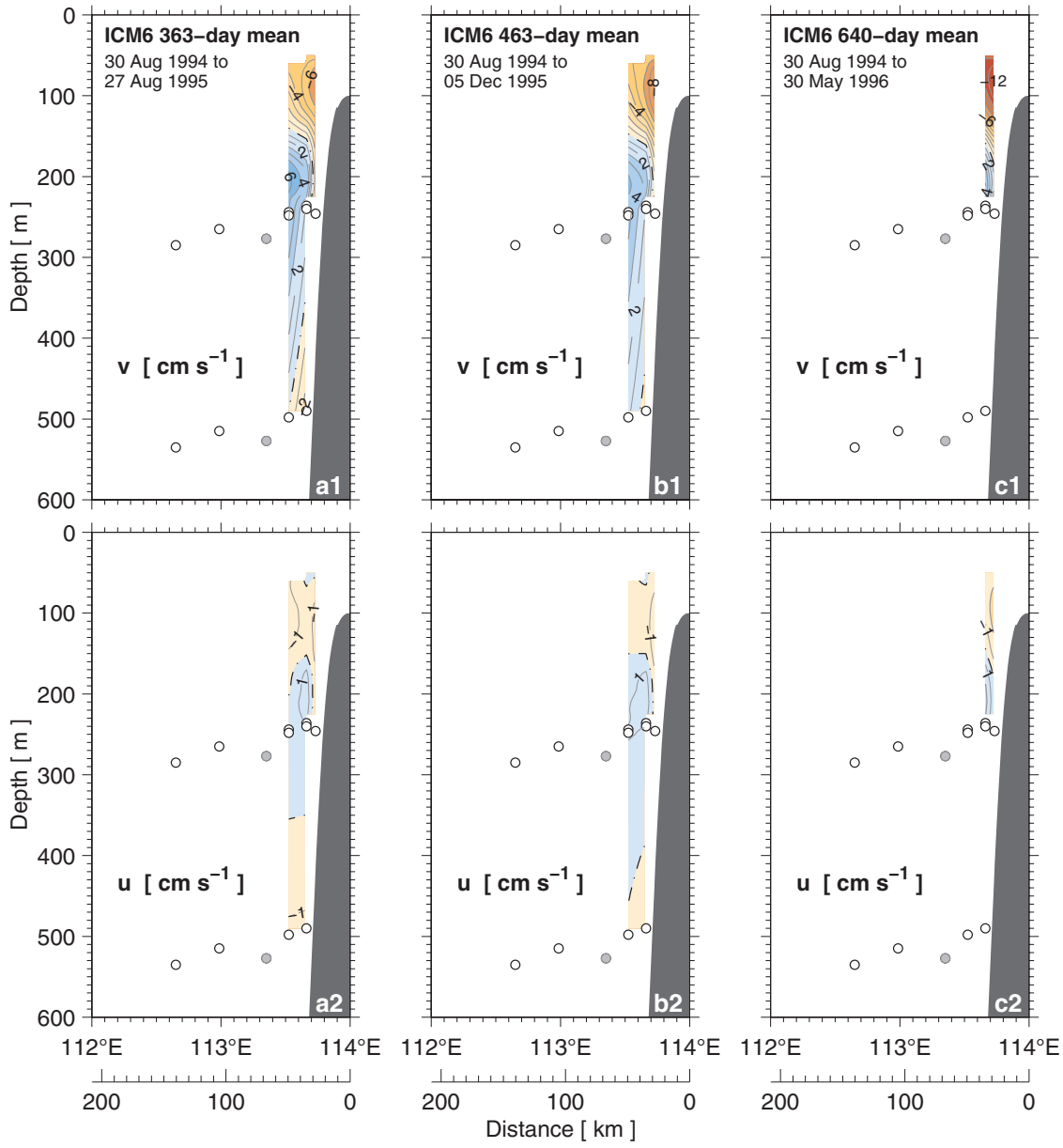

Figure 3.5. ICM6 mean velocity cross–shelf sections (+N,+E). (a) 363–day mean; (b) 463–day mean; and 640–day mean. Circles denote current meters, white (recovered) and gray (not recovered). See text for explanation on the different averaged periods.

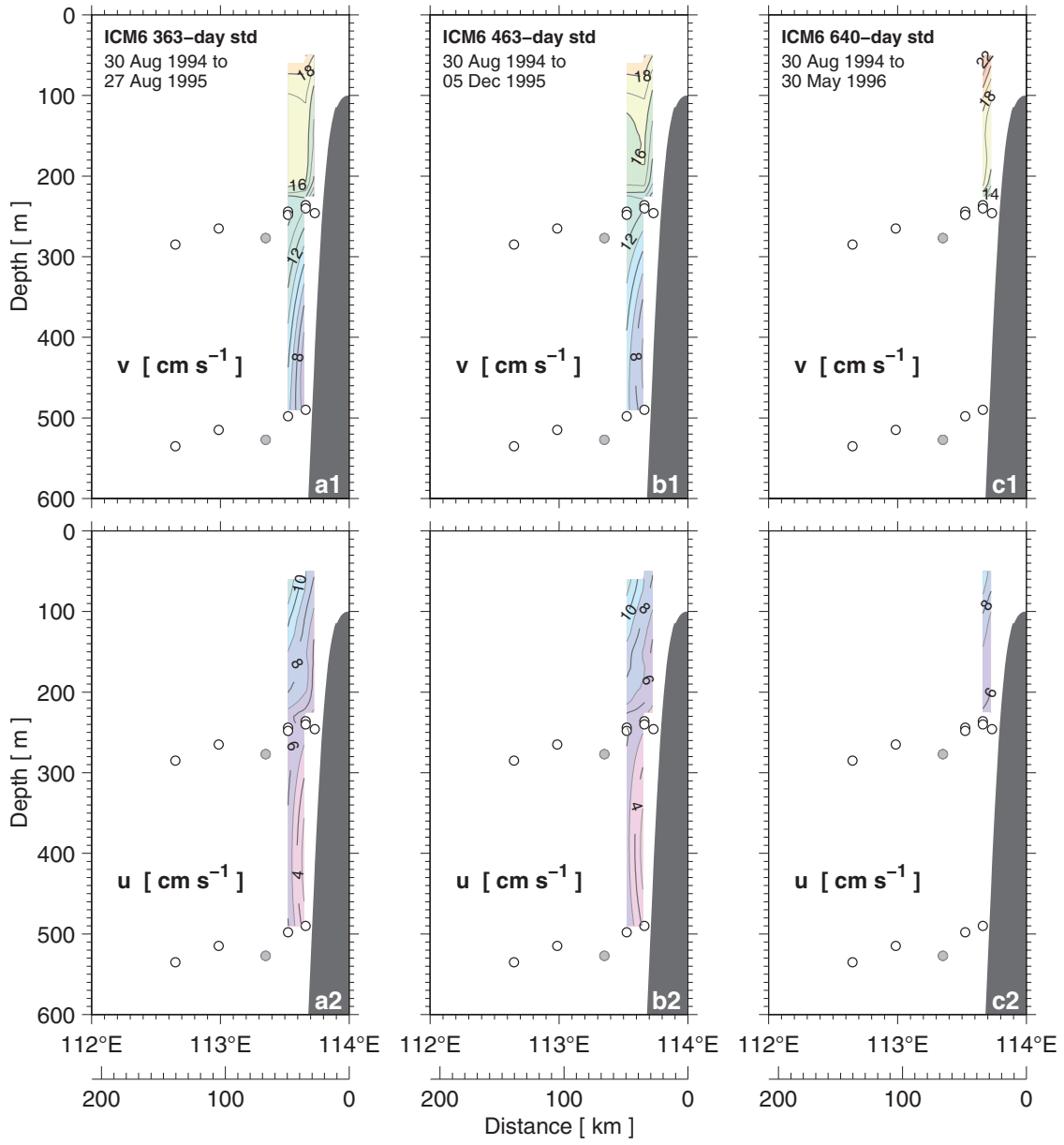

Figure 3.6. ICM6 standard deviation velocity cross–shelf sections (+N,+E). (a) 363–day std; (b) 463–day std; and 640–day std. Circles denote current meters, white (recovered) and gray (not recovered). See text for explanation on the different averaged periods.

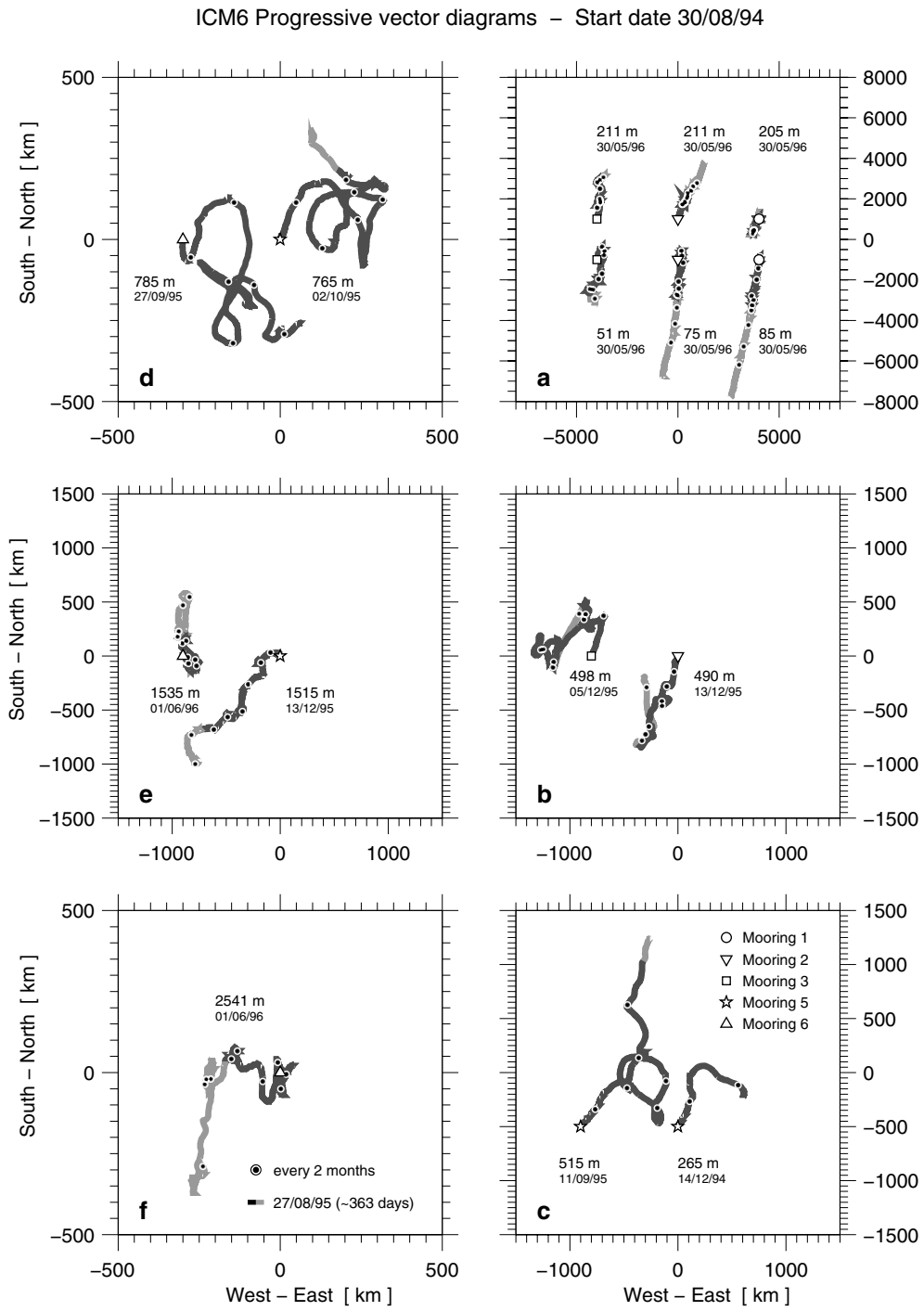

Figure 3.7. ICM6 progressive vector diagrams. Start positions are offset from origin (0,0) in many cases. Start date is 30 August 1994. End dates, moorings and current meter depths are indicated. The gray shade transition marks 30 August 1995 (initial 363 days). White circles indicate a 2–month time step starting from October 1994.

Table 3.3. Statistics of selected ICM6 current meters. Velocity (+N,+E). Note that the number of decimal places is the result of averaging and do not indicate precision.

Current Meter		Record Length			Mean			Standard Deviation		
Mooring	Depth [m]	End Date	N	(Days)	v [cm s^{-1}]	u [cm s^{-1}]	T [°C]	v [cm s^{-1}]	u [cm s^{-1}]	T [°C]
1	85	**27 Aug 95**	**1449**	**(363)**	**-7.06**	**-1.04**	----------	**15.95**	**7.07**	----------
		30 May 96	2557	(640)	-12.31	-2.51	----------	18.43	7.44	----------
1	205/246*	**27 Aug 95**	**1449**	**(363)**	**-1.72**	**-0.77**	**15.24***	**13.61**	**5.39**	**0.84***
		30 May 96	2557	(640)	0.92	0.12	15.57*	15.32	5.76	1.01*
2	75	**27 Aug 95**	**1449**	**(363)**	**-5.37**	**-0.19**	----------	**17.96**	**8.84**	----------
		30 May 96	2557	(640)	-10.43	-1.37	----------	21.01	9.15	----------
2	211/236*	**27 Aug 95**	**1449**	**(363)**	**4.27**	**1.64**	**17.13***	**15.93**	**6.59**	**0.95***
		30 May 96	2557	(640)	5.12	2.38	17.48*	17.27	6.49	1.01*
2	490	**27 Aug 95**	**1449**	**(363)**	**-2.62**	**-1.19**	**8.50**	**6.27**	**3.33**	**0.37**
		13 Dec 95	1881	(471)	-0.51	-0.80	8.57	7.43	3.77	0.38
3	51	**27 Aug 95**	**1449**	**(363)**	**-4.31**	**-1.21**	----------	**19.11**	**12.04**	----------
		30 May 96	2557	(640)	-5.56	-0.28	----------	19.53	11.83	----------
3	211/244*	**27 Aug 95**	**1449**	**(363)**	**6.32**	**0.23**	**17.07***	**16.22**	**7.70**	**0.95***
		30 May 96	2557	(640)	5.65	0.99	17.44*	15.33	7.30	1.00*
3	498	**27 Aug 95**	**1449**	**(363)**	**-0.17**	**-1.19**	**8.58**	**9.28**	**6.11**	**0.46**
		5 Dec 95	1850	(463)	1.14	-0.20	8.71	9.34	6.00	0.49
5	265	14 Dec 94	426	(107)	2.89	6.53	15.85	9.48	7.18	0.53
5	515	**27 Aug 95**	**1449**	**(363)**	**4.90**	**1.86**	**8.43**	**10.03**	**8.19**	**0.66**
		11 Sep 95	1509	(378)	5.34	1.88	8.43	10.17	8.20	0.64
5	765	**27 Aug 95**	**1449**	**(363)**	**0.69**	**0.56**	**5.87**	**4.86**	**3.86**	**0.17**
		2 Oct 95	1593	(399)	0.98	0.31	5.86	4.75	3.88	0.17
5	1515	**27 Aug 95**	**1449**	**(363)**	**-2.16**	**-2.25**	**3.00**	**4.14**	**2.73**	**0.10**
		13 Dec 95	1879	(470)	-2.41	-1.86	3.01	4.10	2.99	0.10
6	285	**27 Aug 95**	**1449**	**(363)**	----------	----------	**16.85**	----------	----------	**0.74**
		1 Jun 96	2563	(641)	----------	----------	17.09	----------	----------	0.76
6	785	**27 Aug 95**	**1449**	**(363)**	**-0.82**	**1.18**	**5.86**	**5.97**	**4.27**	**0.19**
6	1535	**27 Aug 95**	**1449**	**(363)**	**0.61**	**0.00**	**3.34**	**2.98**	**2.76**	**0.10**
		1 Jun 96	2563	(641)	0.54	-0.01	3.34	4.02	2.87	0.11
6	2541	**27 Aug 95**	**1449**	**(363)**	**0.11**	**-0.54**	**2.01**	**2.80**	**1.50**	**0.03**
		1 Jun 96	2563	(641)	-0.57	-0.49	2.00	3.64	1.61	0.04

3.3.1.2 Current and temperature variability

Selected low pass filtered velocity and temperature time series are presented in **Figure 3.8**. Their statistics are listed in **Table 3.3**. The two salient features of the time series are the spatial organisation of the temporal variability of the currents and the long term drifts in temperature. In the current time series, higher frequency signals (flow transitions in a couple of days) prevail near the surface and in the continental slope waveguide, where different classes of trapped waves propagate. Lower frequency signals (flow transitions in a couple of months), such as due to mesoscale eddies, dominate at ~200–800 m depth in the offshore part of the array (moorings 5 and 6). Variance preserving spectra [**Appendix A**], and even a simple visual inspection of the time series, indicate that these offshore variations have a period around 60 to 180 days, consistent with the near semi–annual Rossby waves detected in altimetric studies [Morrow and Birol, 1998]. In the temperature time series, a gradual "cooling" is seen at 2541 m on mooring 6 while a gradual "warming" is apparent in seven out of the thirteen time series. In some of the shorter records and where the eddy–like motion prevails, the warm drift may be obscured. At first glance both warm and cool trends may look suspicious but careful examination suggests they are real features.

It is likely that the warm drift observed in many of the temperature time series is associated with ENSO, and its known response along the western coast of Australia. Previous studies have demonstrated that interannual variability in temperature and in sea level off Western Australia is largely a remote response to ENSO [Pariwono *et al.*, 1986; Pearce and Phillips, 1988; Clarke, 1991; Clarke and Liu, 1994; Meyers, 1996; Potemra and Lukas, 1999; Feng *et al.*, 2003; Wijffels and Meyers, 2004]. The ENSO signal propagates from the tropical Pacific into the southeast Indian Ocean via equatorial Rossby and coastal Kelvin waves. Higher sea level anomalies, warmer sea surface temperatures and deeper thermoclines are expected in a coastally trapped waveguide along the coast during La Niña episodes, and vice–versa for El Niños. During the ICM6 period, ENSO changed phase from an El Niño in 1994 to a La Niña in 1996 (see also Table 2 and Figure 11 in Feng *et al.* [2003]). Thus the warm drifts verified in many of the discrete temperature observations at 22°S can be understood as ENSO driven thermocline deepening. A normalised temperature anomaly Hovmoller constructed from selected current meters at ~200–300 m depth highlights the warming trend and its (informal) correlation with ENSO [**Figure 3.9**]. The SOI adjustment from an El Niño (negative index → cooler water) to a La Niña (positive index → warmer water) is attended by an ongoing temperature warming at depths of the Leeuwin Undercurrent.

An analysis by Wijffels and Meyers [2004], based on ~20 years of Expendable Bathythermograph (XBT) data along the IX–1 and IX–22 lines off Western Australia,

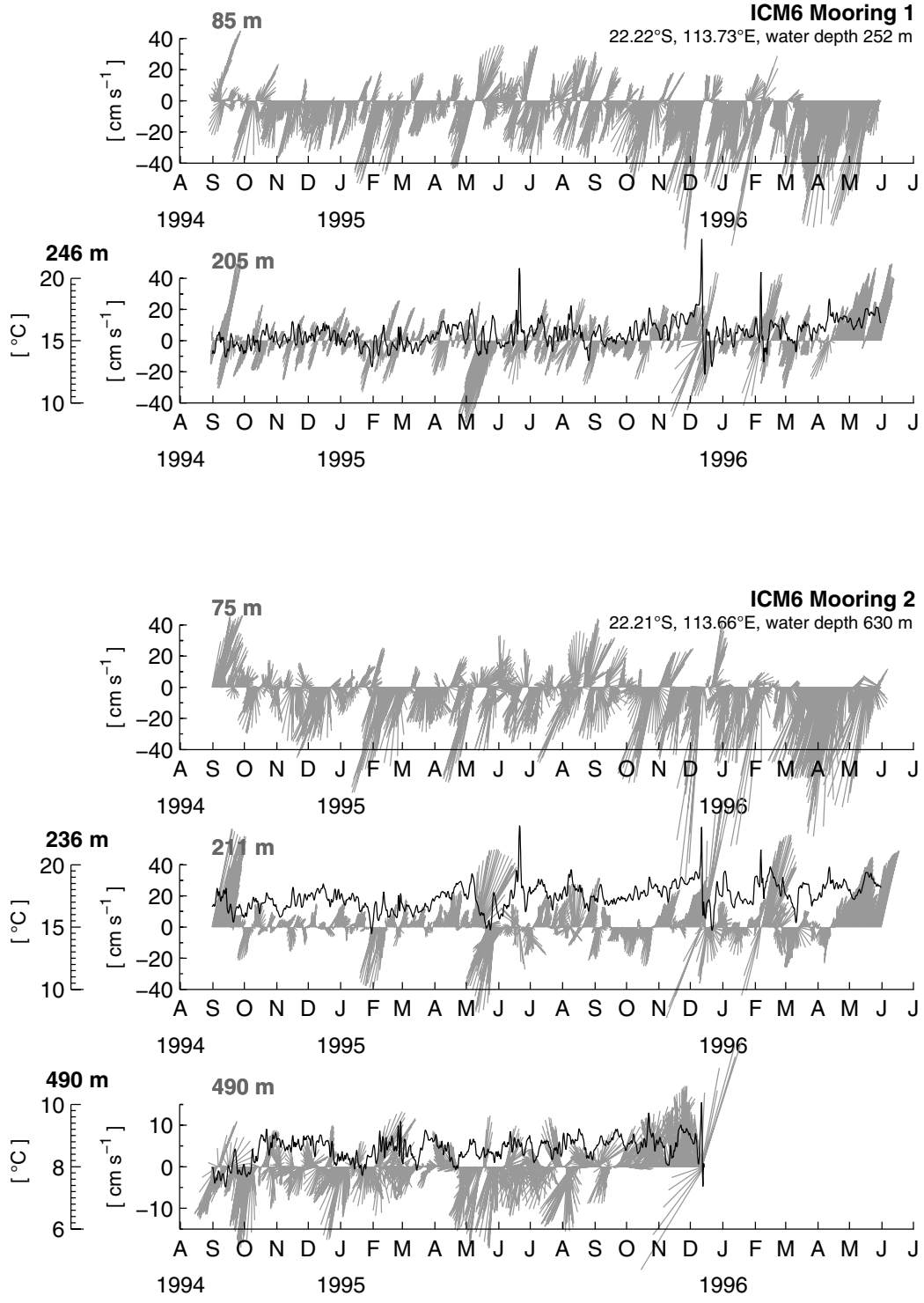

Figure 3.8. ICM6 velocity vectors (+N,+E) and temperature time series.

found an evident interannual signal (> 3.2 years) down to 600 m depth. As the XBT data are limited to those depths, it is not clear how deep in the water column the signal penetrates. The ENSO–related warming in the ICM6 observations reaches to at least 1515 m depth on mooring 5. The deepest current meter, at 2541 m on mooring 6, despite being adjacent to the continental slope and apparently within the coastal waveguide, displays a cooling rather than a warm drift. This cool drift might also be ENSO–linked. According to Clarke and Liu [1994] the ENSO signal is largely explained by the first two baroclinic modes, and a change in sign (or a reverse in temperature trend) at depth is expected.

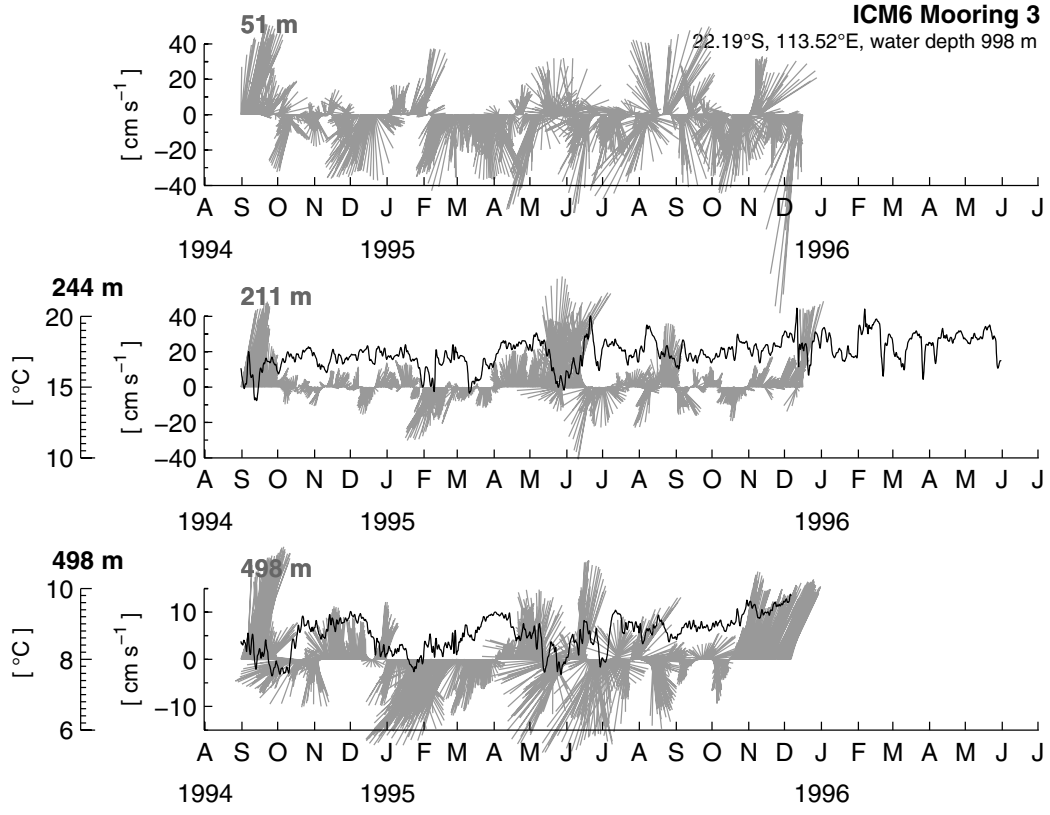

Figure 3.8. ICM6 velocity vectors (+N,+E) and temperature time series. (continued)

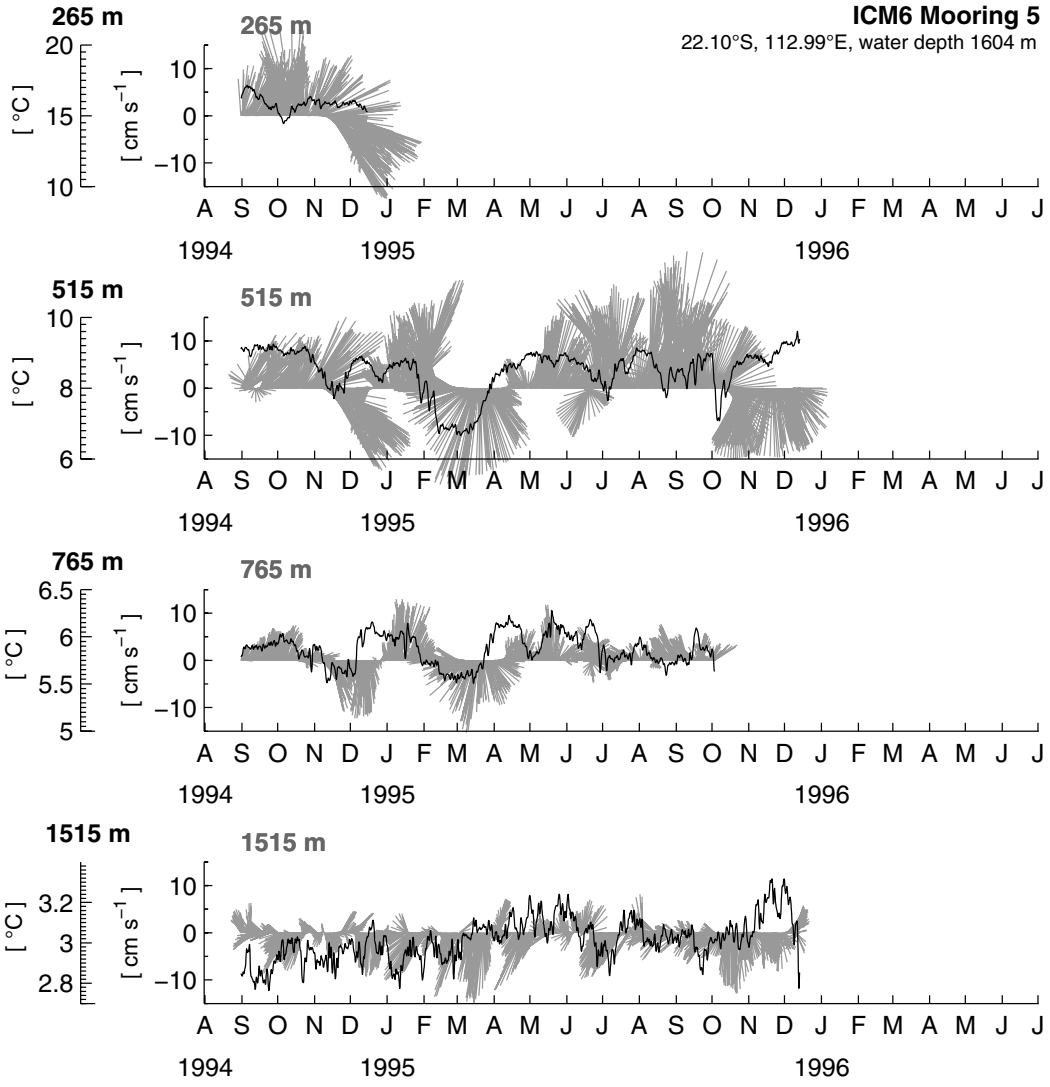

Figure 3.8. ICM6 velocity vectors (+N,+E) and temperature time series. (continued)

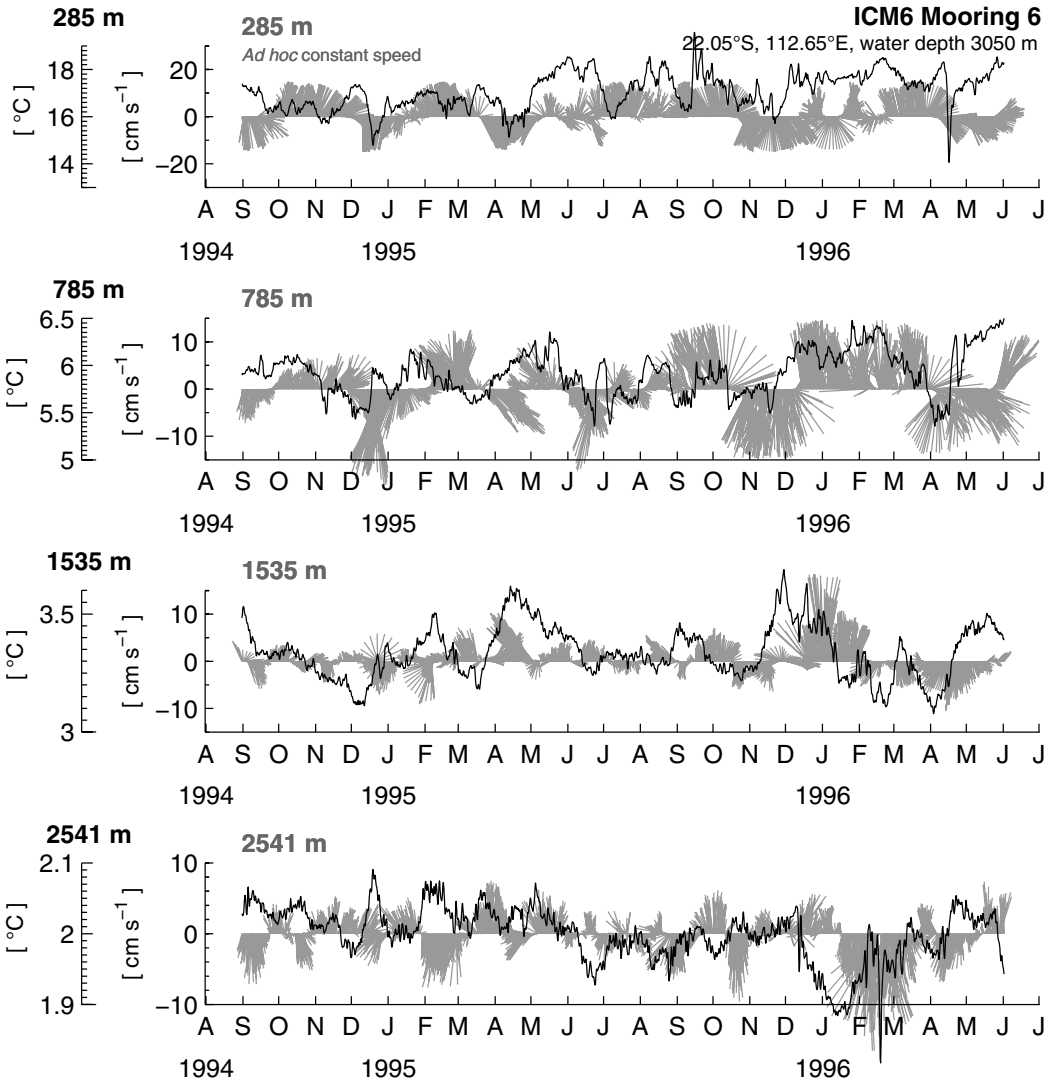

Figure 3.8. ICM6 velocity vectors (+N,+E) and temperature time series. (continued)

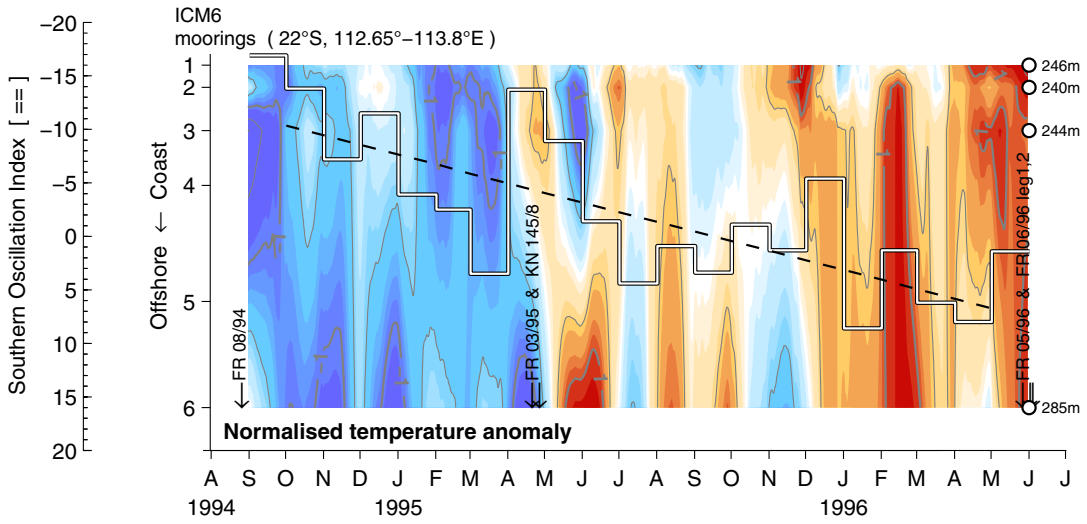

Figure 3.9. ICM6 normalised temperature anomaly Hovmoller at ~200–300 m depth. The monthly averaged SOI is represented by a double thin line and its linear trend over the period by the dashed line. The temperature normalisation was carried out for each instrument to allow intercomparison. Positive anomalies are in red and negative in blue. The anomalies have been smoothed by a 45–day running mean filter. Gray lines outline every 0.5 contour above or below zero.

3.3.1.3 Volume transports

Volume transport time series were formed using the low pass filtered meridional currents from the nearshore part of the array (moorings 1, 2 and 3), multiplied by their respective areas and integrated in depth [**Figure 3.10**]. The depth integration was split based on the 463–day mean picture in terms of Leeuwin Current (v<0) and Leeuwin Undercurrent (v>0) [**Figure 3.5**, panel b1]. The Leeuwin Current time series [top panel] includes velocity extrapolation from the top ADCPs bins to the surface, assuming zero vertical shear in the top 50 m. This time series also contains linearly regressed data to mooring 3 (r.m.s. 0.03 Sv) as indicated by the darker gray shade. A multiple linear regression was additionally attempted but showed no significant improvement. Note that only a narrow part of the Leeuwin Current and an even more marginal portion of the Leeuwin Undercurrent are observed in the direct measurements on moorings 1, 2 and 3. The instruments on mooring 4 were lost or returned bad data whereas on moorings 5 and 6, they were at depths deeper than the Leeuwin Current [see **Table 3.1**].

3.3.1.3.1 Leeuwin Current

Although synoptic variability is not in the scope of this study, fluctuations in the order of one to several weeks are the dominant signal in the low frequency transport time series of the Leeuwin Current [**Figure 3.10**, top panel]. Presumably these fluctuations are created by local wind and/or other remote perturbations, due to coastally trapped waves.

Some of the strongest transient transport maxima were produced by tropical cyclones, which travelled either nearby or directly across the site. Among them, Bobby (25th February) and Frank (11th December) in 1995, and Jacob (5th February), Olivia (10th April) and Jenna (7th May) in 1996. The two largest peaks, –3.5 Sv and –3 Sv, are associated with the passage of Frank and Jacob respectively, both classified as category 3 storms. In an average austral summer, up to six cyclones occur on or near the northwestern coast of Australia and their passage can cause abrupt changes in water properties and in the composition and dispersal of plankton (i.e., fish larvae) communities [McKinnon *et al.*, 2003].

A rather small mean poleward transport of less than –0.3 Sv with no apparent seasonal cycle and large interannual variability are the characteristics of the transport time series. The mean transports for the 363–, 463– and 640–day periods and their standard deviations are detailed in **Table 3.4**, with and without transport extrapolation in the top ~50 m depth (e.g., upper and lower bounds). A maximum poleward value of –0.26 (–0.16) Sv is obtained for the 640–day mean with (without) surface extrapolation. These numbers are very small compared to the mean transport of –3.4 Sv, geostrophically calculated at 32°S from a high resolution regional climatology developed by Feng *et al.* [2003]. Previous annual mean geostrophic estimates in Godfrey and Ridgway [1985] are in a similar range, about –3 to –5 Sv, in the top 300 m at 32.5°S, even though the Leeuwin Current was crudely resolved by their observations at that time.

LUCIE's direct velocity observations at 29.5°S [Smith *et al.*, 1991] are not long enough to examine interannual variability, but their one year long time series suggest that the Leeuwin Current is weak during summer and strong during wintertime. Smith *et al.* did not calculated direct transports but do report on a series of geostrophic estimates obtained from hydrographic observations collected during cruise surveys along the west Australian coast. Overall, their geostrophic values vary from less than –2 Sv in austral summer (February 1987) to more than –5 Sv in autumn and in winter (March, June and August 1987) with intermediate values in early spring (September 1986). Particularly, at 22°S, Smith *et al.* find a poleward transport of –4 Sv in March/June 1987. At this same latitude, however, we have learnt that "instantaneous" geostrophic currents are not reliable, presumably due to large activity of internal waves [Holloway, 1994, 1996; Holloway *et al.*, 2001] which invalidate the thermal wind approximation. All of the adjusted geostrophic shears obtained in cruise surveys across the ICM6 site are unlike the direct observations [Domingues *et al.*, 1999b]. An objective mapping of the hydrographic data, to attenuate ageostrophic noise before the thermal wind calculation, did little to improve the agreement [**Appendix B**].

In addition to quantifying the mean Leeuwin Current at 32°S, Feng *et al.* [2003] also examined seasonal and interannual variability. According to them, the Leeuwin Current first reaches a maximum poleward velocity (–45 cm s^{-1}) in April/May and, after two months, a maximum transport of –5 Sv (June/July). Its annual mean poleward

transport of –3.4 Sv decreases in El Niño years (–3.0 Sv) but increases during La Niña years (–4.2 Sv). At seasonal timescales it is believed that the Leeuwin Current is modulated by a combination of two processes: a remotely forced wave and local wind stress [Godfrey and Ridgway, 1985; Godfrey and Weaver, 1991; Potemra, 2001]. The poleward propagation of an annual Kelvin wave along the west Australian coast [similarly to the interannual wave signal responsible for the ENSO variability mentioned in **Section 3.1.2**] is positively reinforced by a minimum in the local equatorward wind stress (e.g., see **Figure 2.5**). This combination would then give rise to a seasonally stronger Leeuwin Current during late autumn, early winter.

The Leeuwin Current volume transport time series from ICM6 suggests interannual variability but it does not indicate any clear seasonal modulation. A maximum poleward transport of –1.1 Sv is seen in April 1996 but not in April 1995. Weak transport is not verified in summer months, December/January/February 1995 and 1996, but it is in wintertime, from April to September 1995. The only aspect of the series that apparently agrees with the literature is the ENSO variability, associated with an increase in the poleward transport of the Leeuwin Current in 1996, a La Niña year. As pointed out in **Section 3.1.1**, the Leeuwin Current axis often meanders out of the array limits, so the ICM6 direct observations not only underestimates the mean transport of the current but in some ways can also misrepresent its low frequency variability. This shortcoming may explain the lack of a clear seasonal cycle.

Table 3.4. Mean and standard deviation of the Leeuwin Current's volume transport (+N,+E), with and without surface extrapolation (no vertical shear) in the top 50 m to provide an upper and lower bound to the estimates.

Record Length		Transport [Sv]			
End Date	N (Days)	NO Surface Extrapolation		Surface Extrapolation	
		Mean	STD	Mean	STD
27 Aug 95	1449 (363)	-0.09	0.35	-0.14	0.53
5 Dec 95	1850 (463)	-0.11	0.35	-0.17	0.53
30 May 96	2557 (640)	-0.16	0.38	-0.26	0.59

3.3.1.3.2 Leeuwin Undercurrent

Due to current meter failures the transport time series of Leeuwin Undercurrent is shorter than for the Leeuwin Current [**Figure 3.10**, bottom panel]. Monthly mean equatorward maxima are seen in September 1994 (1 Sv), April 1995 (0.4 Sv) and November 1995 (0.5 Sv), nearly every 120 days. The series only resolves the undercurrent's inner flank [see **Figure 3.5**], so its mean estimate is small, 0.11 Sv. Steric height maps (450/700 dbar) in Godfrey and Ridgway [1985] suggest an annual mean

transport of 1 to 2 Sv at 32°S. Smith *et al.* [1991] do not provide a transport estimate for their marginally resolved undercurrent at 29.5°S. After suspending a current meter during a cruise in May 1982, Thompson [1984] estimates it carries 5 Sv at ~300 m depth, between 22° and 24°S. Near Cape Mentelle (34°S), Cresswell and Peterson [1993] observed an undercurrent with a geostrophic transport of ~2.9 Sv, between 200–800 m, in June 1987. Although transport snapshots of the Leeuwin Undercurrent are widely available, a long term mean estimate lacks.

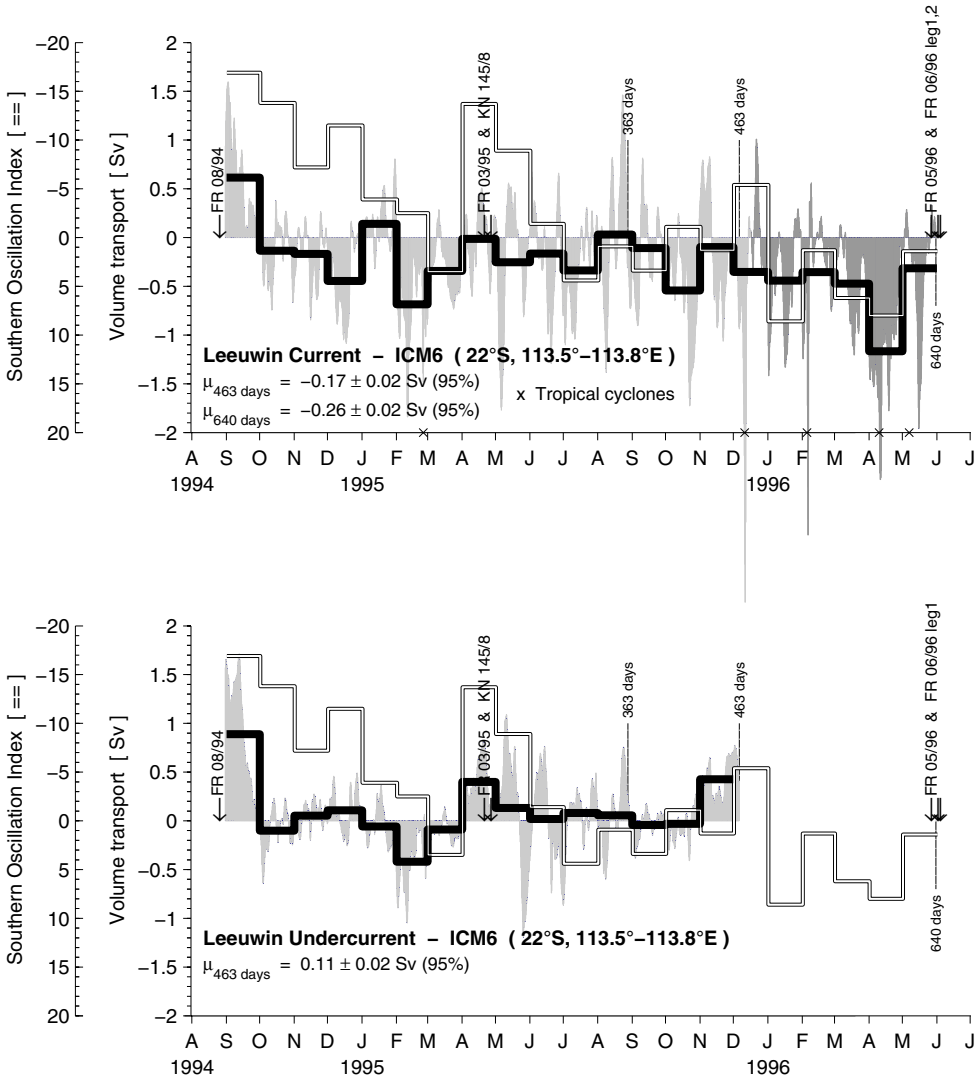

Figure 3.10. ICM6 volume transport time series (+N,+E). Leeuwin Current (top) and Leeuwin Undercurrent (bottom). Low frequency variability is in gray. Its darker segment includes linearly regressed data on mooring 3. The thick black lines are monthly averaged transports while double thin lines are monthly averaged SOI. Cruise dates are marked by arrows and some calendar dates are outlined by vertical dashed lines. Tropical cyclones dates (x) are indicated on top of the timeline axis. The long term means and their error estimates are indicated (bottom left corner).

3.3.2 Shipboard ADCP currents

The highly variable temporal and spatial nature of the near surface velocity field is verified in the SADCP sections [**Figure 3.11**], even when cruise legs are not far apart in time, such as during June 1996 [panels e and f]. While the Leeuwin Current is not always clearly present, a steadier Leeuwin Undercurrent may be recognised with an equatorward maximum over the upper continental slope around 200–300 m depth. Good agreement between the SLA inferred velocity anomaly field – (anti) clockwise flow around (high) low SLAs as required by thermal wind balance in the southern hemisphere – and the SADCP vectors in **Figure 3.12** implies that large scale geostrophy [e.g., eddy field] plays an important role. Some of the differences among the fields may be explained in terms of comparison of non–simultaneous data of uneven spatial resolution as well as by the assumption that the 20–m SADCP vectors are an equivalent indicator of the flow pattern inferred from SLA.

In August 1994 and April 1995, the Leeuwin Current jet is moving poleward with velocities up to 30 to 40 cm s^{-1} along steep sea level slopes, associated with the western rim of positive SLAs [**Figures 3.12, 3.13** and **3.14**], near moorings 5 and 6. In August 1994, the jet is disrupted by a mushroom–like meandering, with an anticyclonic motion (positive SLA) inshore of mooring 6 and a cyclonic motion offshore (negative SLA). The larger SLA map suggests water transport from tropical latitudes of the open ocean – from north of 17°S and centred at 110°E.

In April 1995, the poleward jet of the Leeuwin Current meanders seaward around an anticyclone to the south which causes a counter flow closer to the coast during days 21–22 [**Figures 3.12, 3.13** and **3.14**]. The SST image shows that the counter flow apparently draws cold water from the shelf. During days 26–27, this picture is substituted by poleward flow. The larger SLA maps depict a continuously coastally trapped positive SLA at least from 18°S, indicating a possible inflow into the Leeuwin Current from the tropical area just off the southern part of the North West Shelf. The continuously coastally trapped positive SLA is most likely a response to the poleward propagation of the annual Kelvin wave that partially contributes to the modulation of the Leeuwin Current's seasonal cycle [Godfrey and Ridgway, 1985].

SST images from August 1994 and April 1995 [**Figure 3.14**, panels a,b] reveal meandering of the Leeuwin Current jet away from the ICM6 site. They also show that the jet is embedded in a broad raft of warm surface water which only takes the form of a narrower stream–like feature south of 22°S. As for the SST image in May/June 1996 [panel c], a narrow warm stream is well defined at the array location, with a broad patch of warm surface water sitting immediate to its north. This broad patch is associated with a positive SLA [**Figure 3.12**, panels c1,c3]. Initially, on 27–28th May, the southern rim of

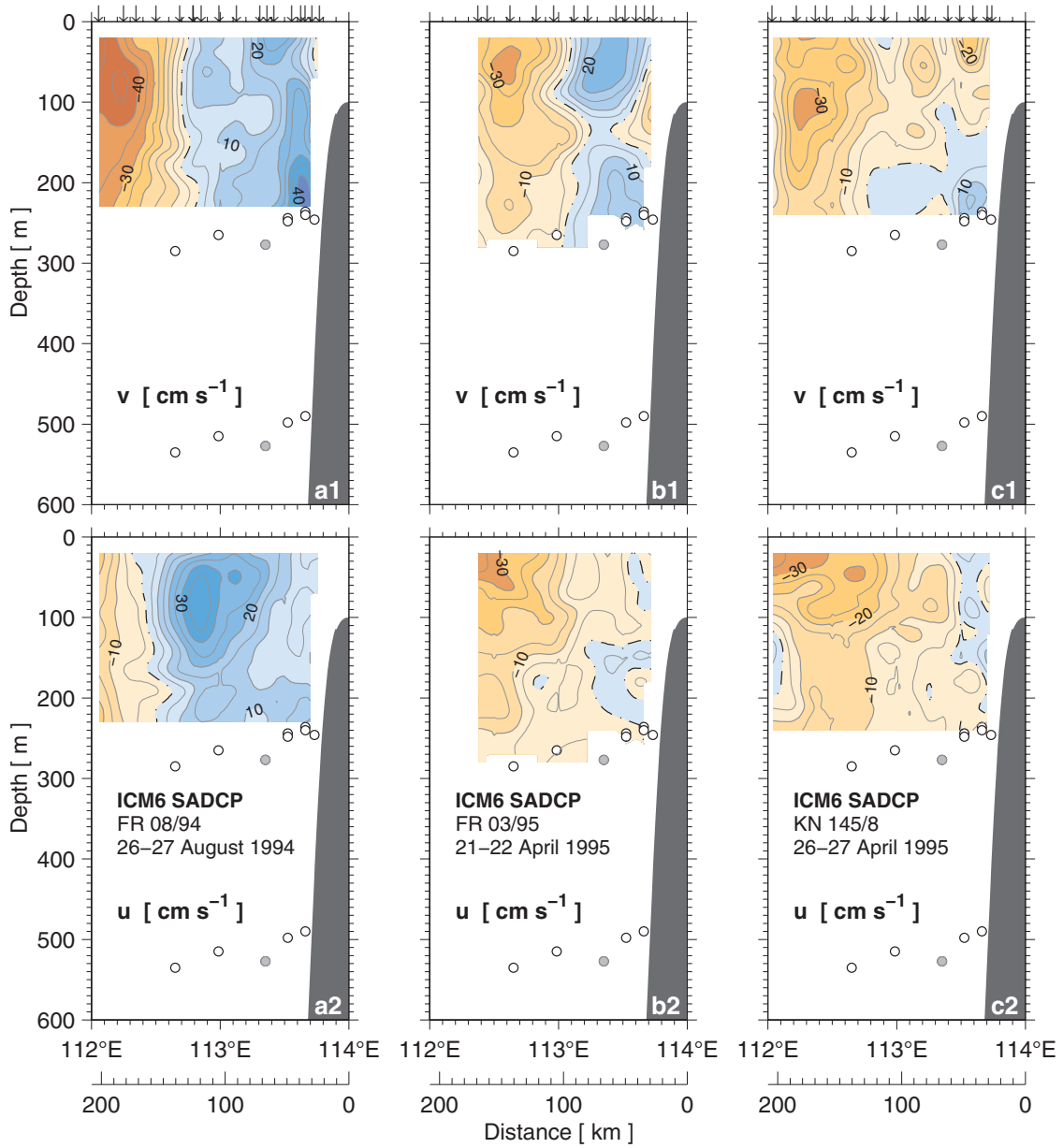

Figure 3.11. SADCP upper ocean velocity (+N,+E) sections for individual cruise surveys across the ICM6 array, as indicated. Circles denote current meters, white (recovered) and gray (not recovered).

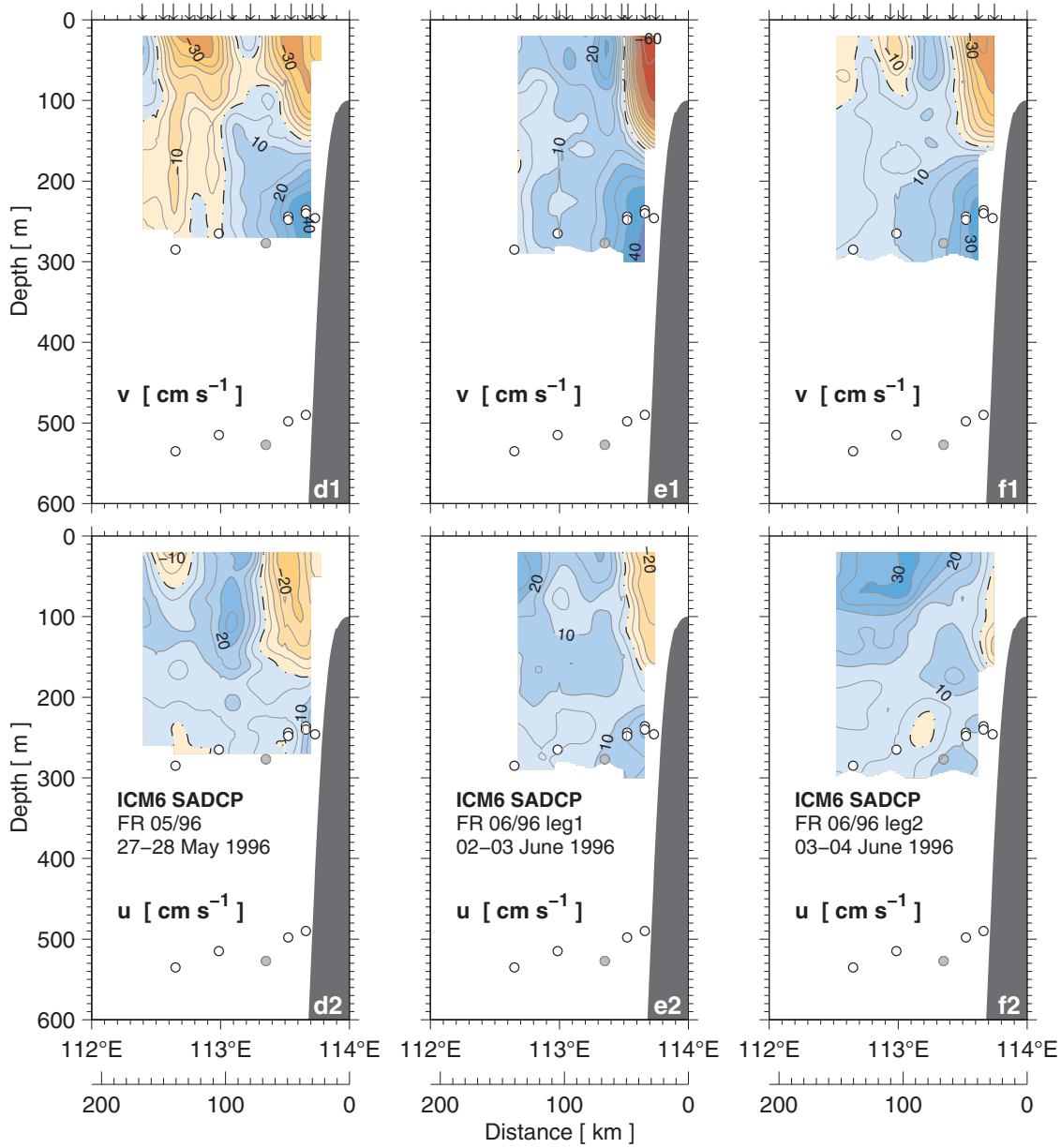

Figure 3.11. SADCP upper ocean velocity (+N,+E) sections for individual cruise surveys across the ICM6 array, as indicated. Circles denote current meters, white (recovered) and gray (not recovered). (continued)

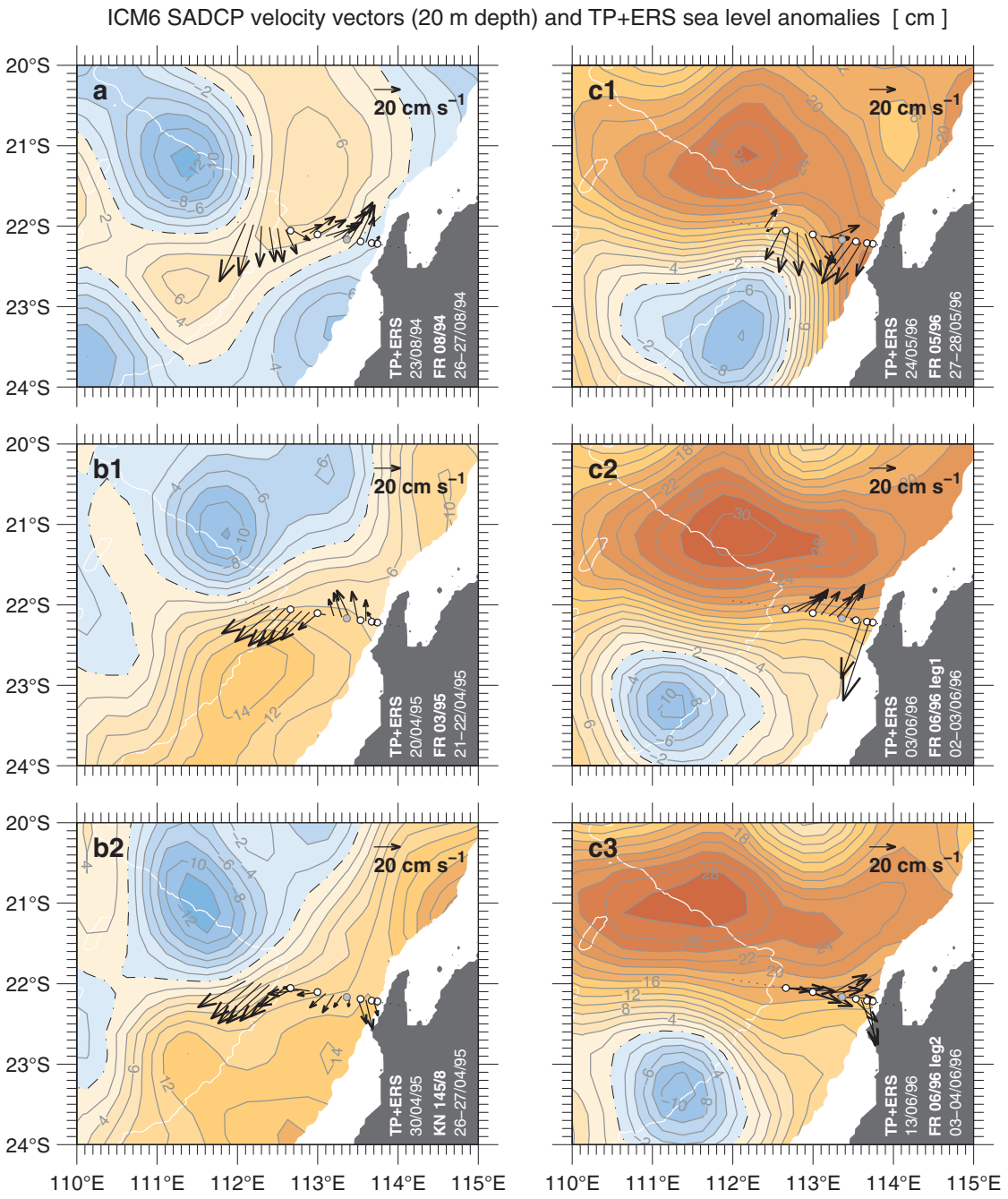

Figure 3.12. ICM6 SADCP 20–m vectors overlain in TP+ERS maps of sea level anomaly for individual cruise surveys across the ICM6 array, as indicated. Map dates are as close as possible to ICM6 cruise dates [**Table 3.2**]. Circles denote current meters, white (recovered) and gray (not recovered). The white line is the 4000 m isobath. A large scale version of these maps (15° to 35°S) are shown in **Figure 3.13**.

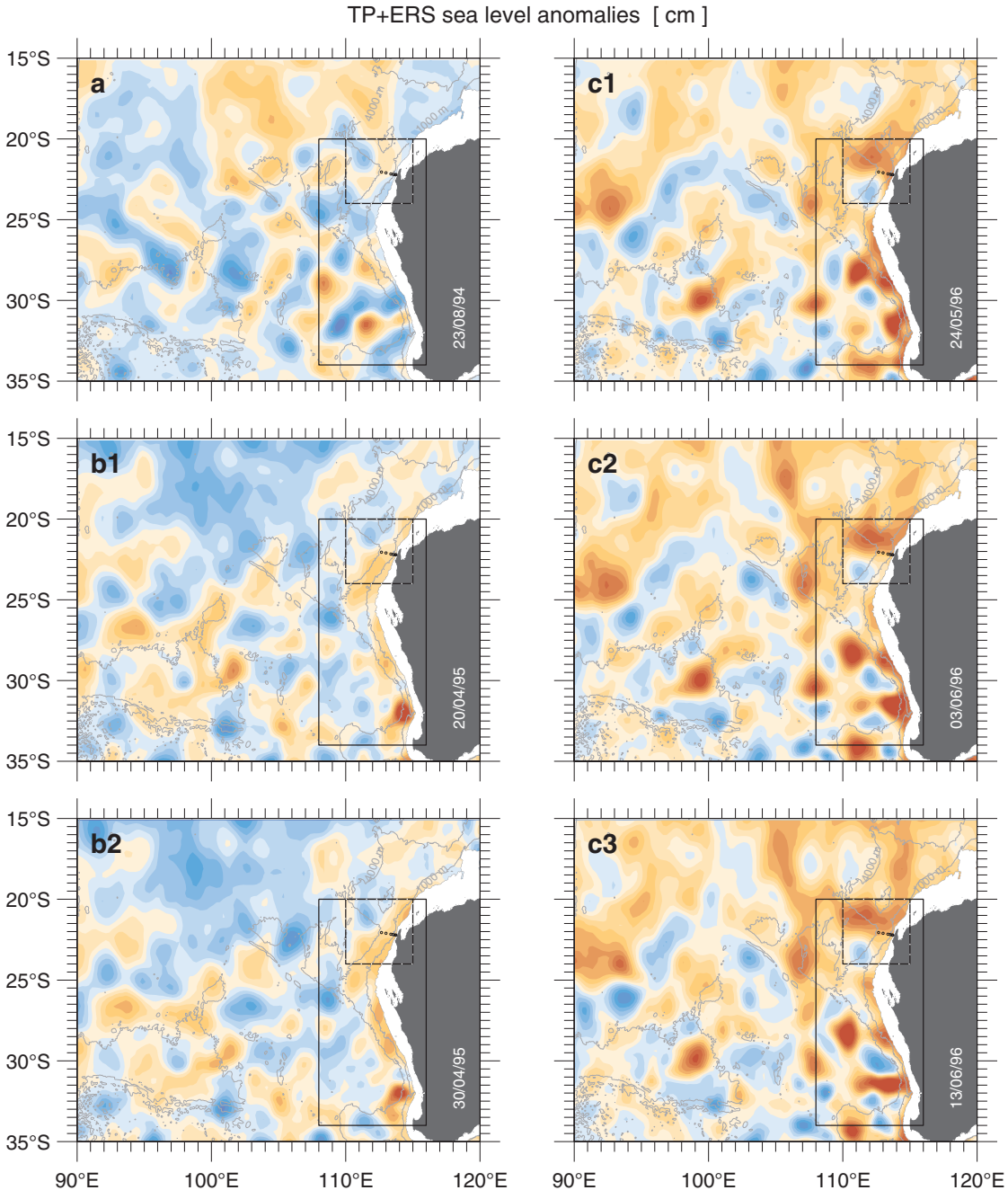

Figure 3.13. TP+ERS maps of sea level anomaly in a large scale version. Circles denote ICM6 moorings, the smaller rectangle (dashed line) is the area shown in **Figure 3.12** and the larger rectangle (solid line) is the area shown in **Figure 3.14**. Isobaths (gray lines) are 1000 and 4000 m.

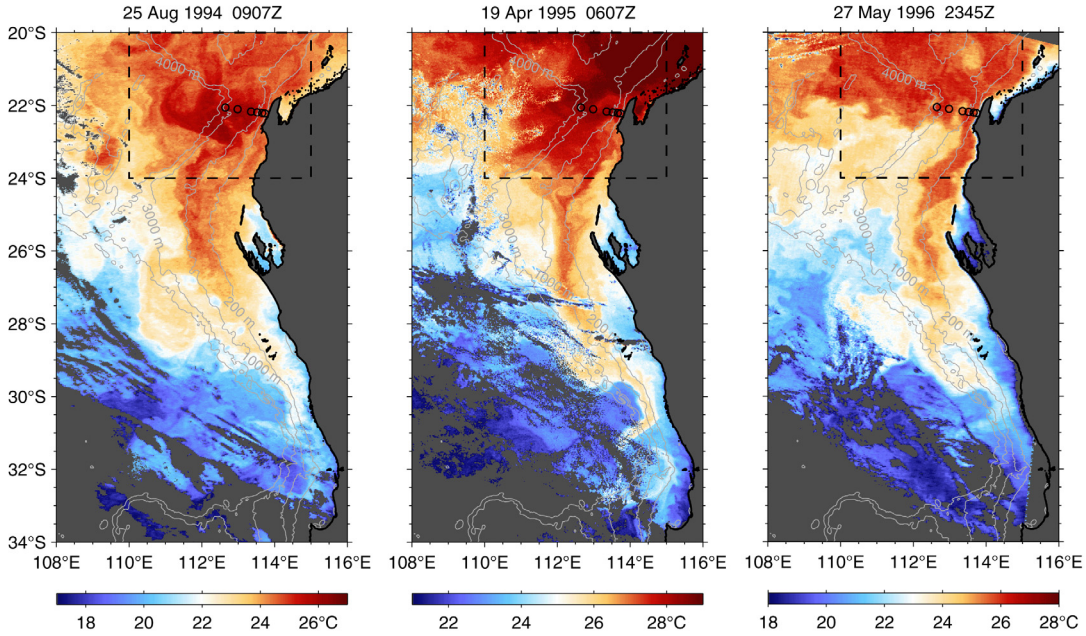

Figure 3.14. Sea surface temperature images. Circles denote ICM6 moorings and the dashed rectangle is the area shown in **Figure 3.13**. Image dates are as close as possible to the ICM6 cruise dates [**Table 3.2**]. Isobaths (gray lines) are 200, 1000, 3000 and 4000 m. Gray shades over ocean are clouds.

this SLA, delimited by a thermal front in the SST image, gives rise to an onshore flow that veers poleward just over the ICM6 site. Subsequently, on 2nd–3rd June, the SLA starts to detach from the coast and to move westward, favouring an equatorward flow offshore mooring 3. However, although not captured by the SLA map, a narrow and swift poleward jet of –60 cm s^{-1} persists in shallower waters. By the time of the last snapshot, on the 3rd–4th June, the situation reverses to a predominant onshore flow that apparently brings warm water from the open ocean into the coastal poleward jet of the Leeuwin Current, presently with a maximum speed of –30 cm s^{-1}. South of 22°S, part of this warm water invades the west Australian continental shelf, creating a thermal front with the cooler coastal waters. The shelf invasion by waters of the Leeuwin Current is observed in all of the three SST snapshots and, in fact, is typical of numerous SST images (not shown), most commonly in autumn/winter.

Overall, the synoptic observations reveal that the Leeuwin Current is usually embedded in a broad raft of warm tropical water, which tapers into a more defined jet either at 22°S or further south along the coast. The near surface waters crossing the ICM6 site are potentially drawn from a coastally trapped flow along the southern part of the North West Shelf region and also from the offshore tropical open ocean. This snapshot picture agrees with previous qualitative sketches of the surface circulation inferred from extensive satellite imagery [Pearce, *pers. comm.*] and historical XBT observations [Gentilli, 1972; Meyers *et al.*, 1996; Wijffels *et al.*, 1996].

3.3.3 Water properties

The property distributions obtained during the cruise surveys across the ICM6 site at 22°S [**Figures 3.15** to **3.20**] show the water column to be well divided in terms of salinity and to mainly consist of:

i. a near surface layer of comparatively warm fresh water
   $S < 35.4$ psu; $\theta \geq 20$°C; $\sigma_\theta \leq 24.8$ kg m^{-3} in the top ~150–200 m depth

ii. a salinity maximum
   $S \geq 35.6$ psu; $\theta \approx 18$°C; $\sigma_\theta \approx 25.8$ kg m^{-3} at ~200–300 m depth

iii. a maximum to minimum salinity layer
   $34.7 \leq S \leq 35.4$; $9° \leq \theta \leq 15$°C; $26.2 \leq \sigma_\theta \leq 26.9$ kg m^{-3} at ~400–500 m depth

iv. a salinity minimum
   $S \leq 34.6$ psu; $\theta \approx 6.8$°C; $\sigma_\theta \approx 27.1$ kg m^{-3} at ~600–800 m depth

v. a near isohaline layer
   $34.61 \leq S \leq 34.64$; $3.5° \leq \theta \leq 6$°C; $27.3 \leq \sigma_\theta \leq 27.5$ kg m^{-3} at ~900–1400 m depth

vi. a minimum to maximum salinity layer
   $34.65 \leq S \leq 34.69$; $\theta \approx 3.2$°C; $\sigma_\theta \approx 27.65$ kg m^{-3} at ~1500–1800 m depth

vii. a deep salinity maximum
   $S \geq 34.7$ psu; $\theta \leq 2.5$°C; $\sigma_\theta \geq 27.7$ kg m^{-3} at ~2000–2200 m depth

The nomenclature adopted for the water properties follows their θ–S diagrams [**Figure 3.21**]. The fresher and warmer near surface water is Tropical Water (TW). Subtropical Water (STW) is represented by the salinity maximum of ~35.8 psu whereas the salinity minimum of ~34.5 psu defines Antarctic Intermediate Water (AAIW). Below the STW salinity maximum and above the AAIW salinity minimum, an almost linear θ–S relationship depicts South Indian Central Water (SICW). As Subantarctic Mode Water (SAMW) and the lower end of SICW share the same θ–S profile, other tracers such as oxygen and potential vorticity, are needed for their separation. A deep salinity maximum of ~34.72 psu is linked with Indian Deep Water (IDW), also referred as Circumpolar Deep Water in some work. At lighter densities than IDW, but at the same or somewhat higher densities of AAIW, a near isohaline water distribution is identified. It is not exactly clear how to term this water but it is referred as Mixed Intermediate Water (MIW) hereafter.

3.3.3.1 Variability between cruise surveys

The cross–shelf sections show how the water column across ICM6 differs between surveys [**Figures 3.15** to **3.20**]. The SST displays the expected seasonal cycle: coolest in August (24°C), warmest in April (27–28°C) and slightly cooler in May/June (26°C). In August 1994, a fresh salinity cap lies in the upper 50 m and weak temperature stratification is found in the top 150 m. In April 1995, a subsurface lens of low salinity (≤35.2 psu, 50–100 m), just below the mixed layer (~50 m), is interposed in more saline water. In May/June 1996, a deepening of the seasonal (pycnocline) thermocline, most intense near the shelf break, is marked by a strong downward slant. TW spans a far more impressive area, with salinities as low as 34.81 psu in the seaward side of the section. Its upper limit lies within the mixed layer, ~100 m deep inshore but less than 70 m offshore, while its lower limit intrudes into the seasonal (pycnocline) thermocline. Variations in TW are detected in θ–S space [**Figure 3.21**]. In May/June 1996 [panel c], TW is depicted by two profiles. One, in which temperature varies along a near constant salinity of 34.9 psu, and another, which form is akin the profile from August 1994 [panel a]. An "intermediate" profile is deemed for April 1995 [panel b], ignoring the saline cap. Interleaving between the different TW profiles and, also between TW and STW, appears to be common (e.g., small scale salinity intrusions in the cross–shelf sections). In fact, interleaving is a widespread feature. At deeper levels, it is associated with SICW, AAIW and MIW.

Processes operating on seasonal and interannual timescales are likely to explain in great part the different θ–S profiles observed for TW at 22°S. Monthly θ–S diagrams constructed from CARS across 20°S (103°–120°E), immediately north of ICM6, illustrate how the TW curve associated with the bluish colours (110°–114°E) varies during the seasons [**Figure 3.22**]. It depicts a near linear θ–S relationship from June to November, however, from December to May, an extra slant develops on its top. The near isohaline curve of low salinity seen in May/June 1996 is presumably due to advection of TW from the northeast of ICM6 (hot colours), as this characteristic is not present to the northwest of the site (cool colours). At interannual scales, Phillips *et al.* [2005] show the freshwater content in the upper 200 m of the ocean, between Australia and Indonesia, to substantially differ from the annual mean CARS climatology. While TW became fresher, STW became more saline. This change was trigged during an unusually long La Niña and persisted for ~2 years (1998/00). The ICM6 May/June 1996 snapshot is from a La Niña year, and similar conditions, such as fresher TW and more saline STW, are also apparent.

At thermocline and intermediate depths, variability is evident if we compare the cross–shelf sections from 1994/95 with 1996. The 35.8 salinity core (maximum of 35.92 psu) of STW, the low AAIW salinity core (minimum of 34.47 psu) delimited by the 34.6 isohaline, and the deeper 34.61–34.63 salinity layer of MIW are all more robust in 1996.

Inspection of the 35.6, 34.6 and 34.63 contours imply that their respective lower bounds are consistently displaced to greater depths. STW has its salinity maximum eroded in 1994/95, is relatively warmer in April 1995 than in August 1994, and is warmest and most saline during May/June 1996. While AAIW and MIW reach their lowest salinities in May/June 1996, the highest ones are found in April 1995. In addition, an extended isohaline profile of MIW in the θ–S diagram [**Figure 3.21**, panel b] clearly straddles the same isopycnal layer of the AAIW core.

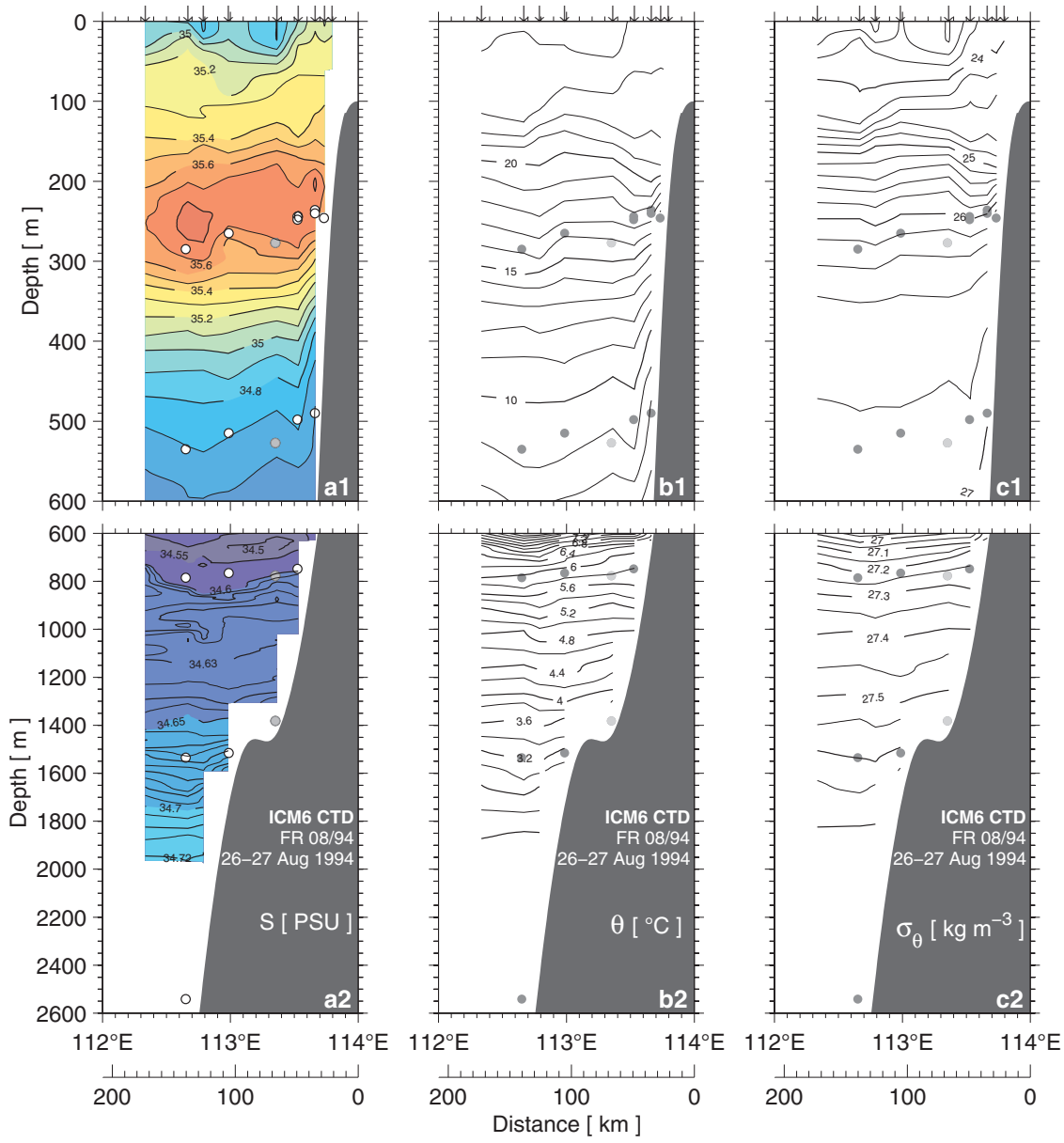

Figure 3.15. ICM6 Hydrographic sections during voyage FR 08/94. The section is split in upper (1) and deeper (2) ocean. Circles denote current meters, white (recovered) and gray (not recovered). CTD stations are indicated by downward pointing arrows.

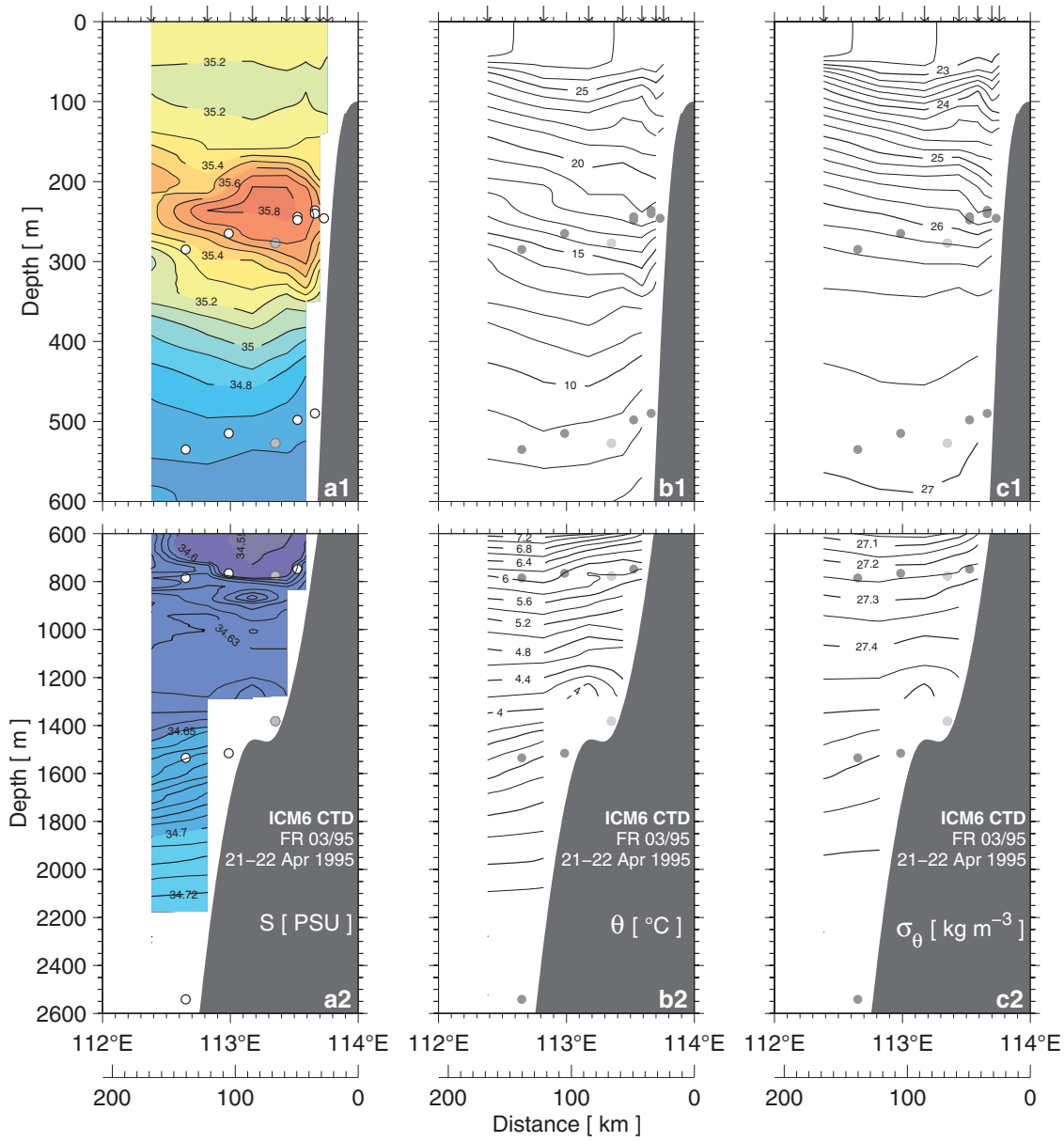

Figure 3.16. ICM6 Hydrographic sections during voyage FR 03/95. The section is split in upper (1) and deeper (2) ocean. Circles denote current meters, white (recovered) and gray (not recovered). CTD stations are indicated by downward pointing arrows.

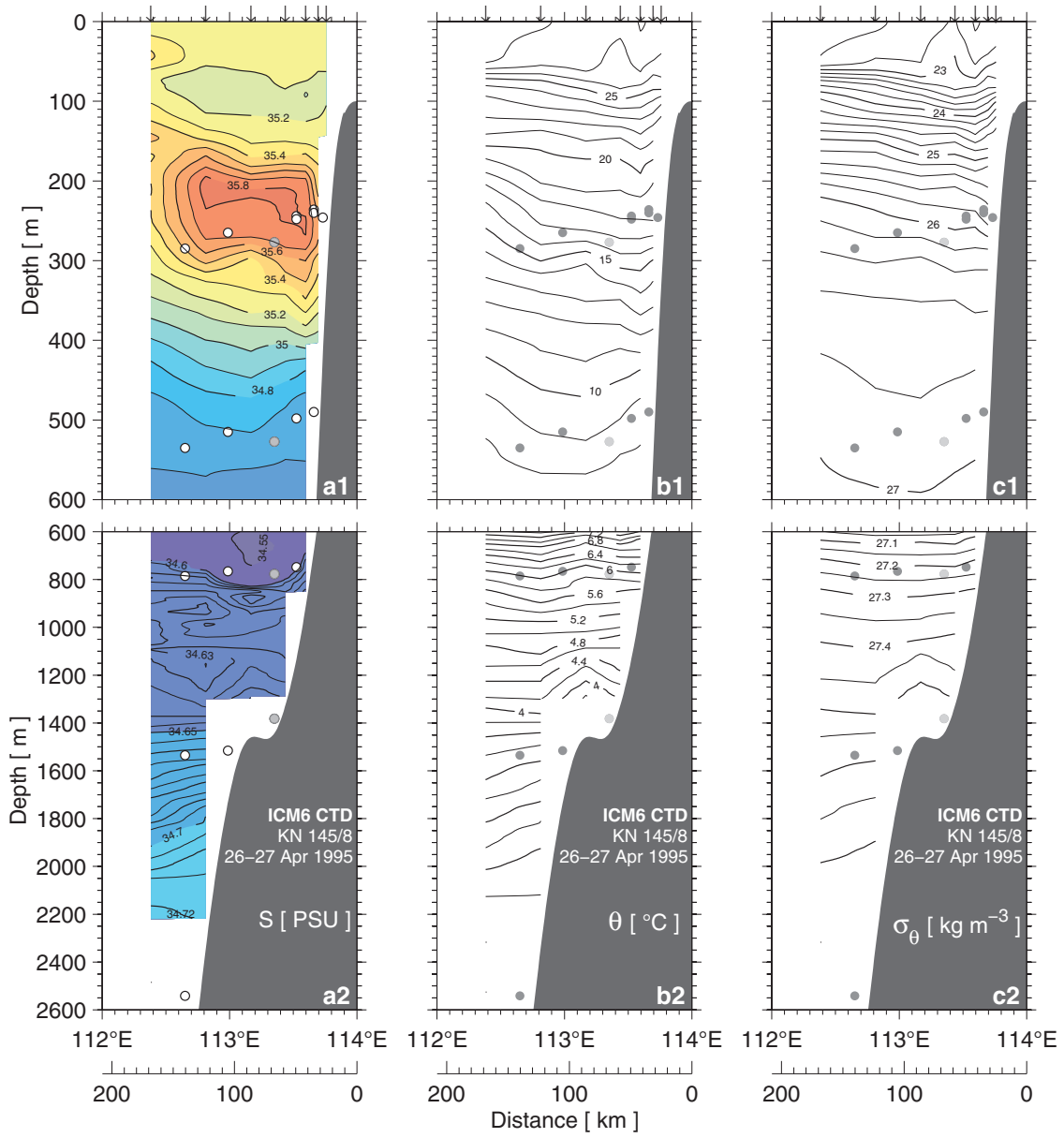

Figure 3.17. ICM6 Hydrographic sections during voyage KN 145/8. The section is split in upper (1) and deeper (2) ocean. Circles denote current meters, white (recovered) and gray (not recovered). CTD stations are indicated by downward pointing arrows.

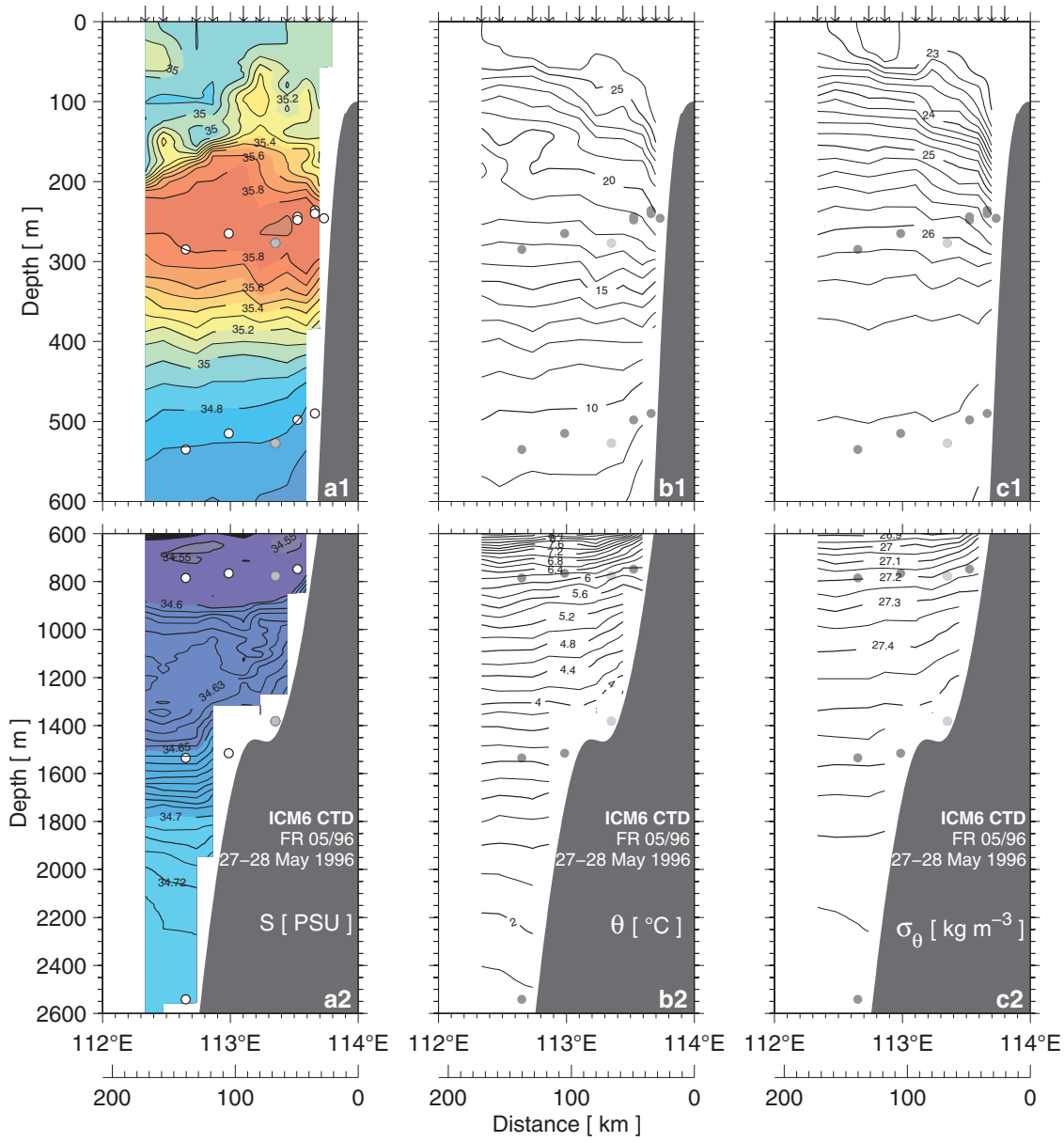

Figure 3.18. ICM6 Hydrographic sections during voyage FR 05/96. The section is split in upper (1) and deeper (2) ocean. Circles denote current meters, white (recovered) and gray (not recovered). CTD stations are indicated by downward pointing arrows.

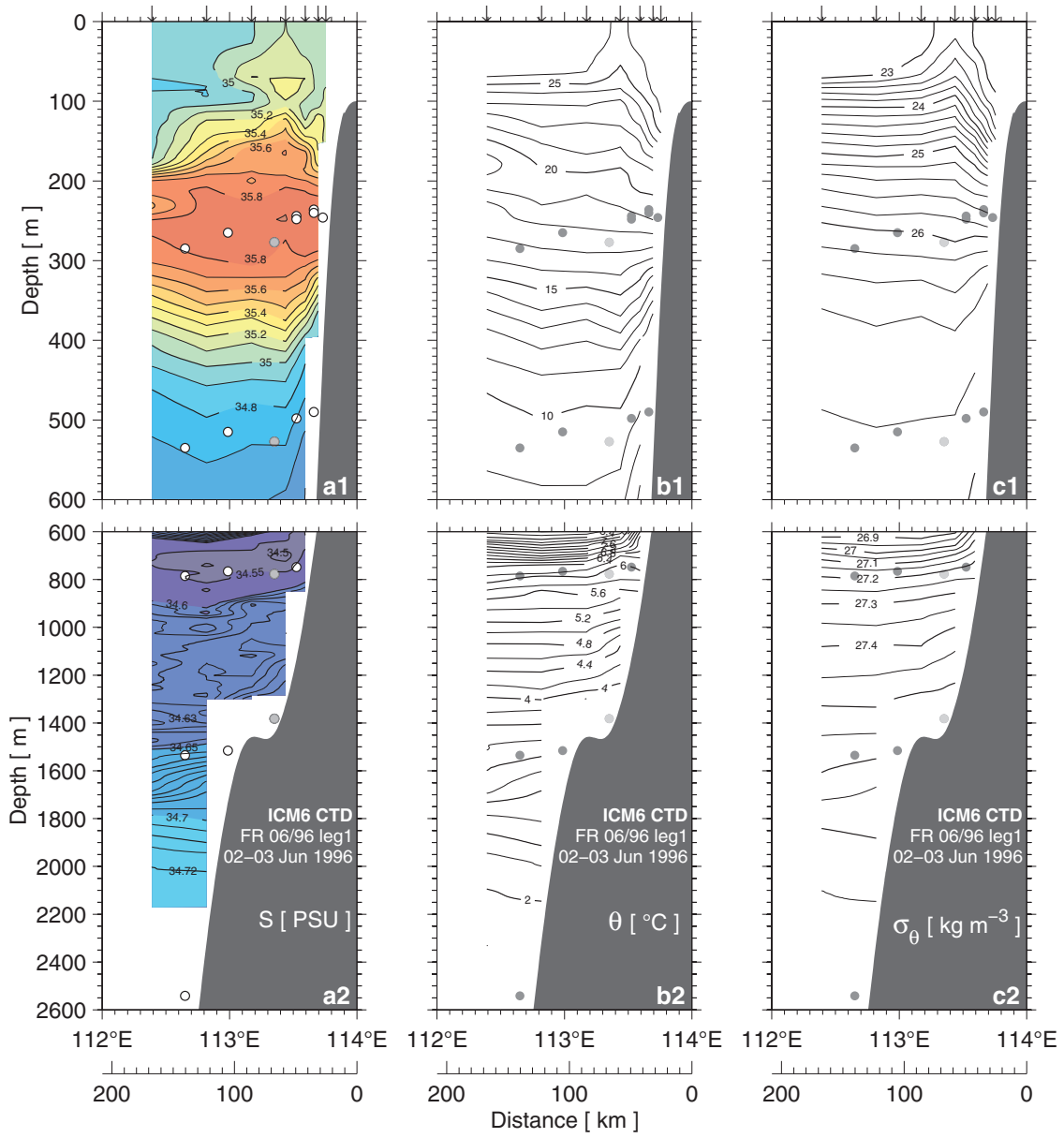

Figure 3.19. ICM6 Hydrographic sections during voyage FR 06/96 leg1. The section is split in upper (1) and deeper (2) ocean. Circles denote current meters, white (recovered) and gray (not recovered). CTD stations are indicated by downward pointing arrows.

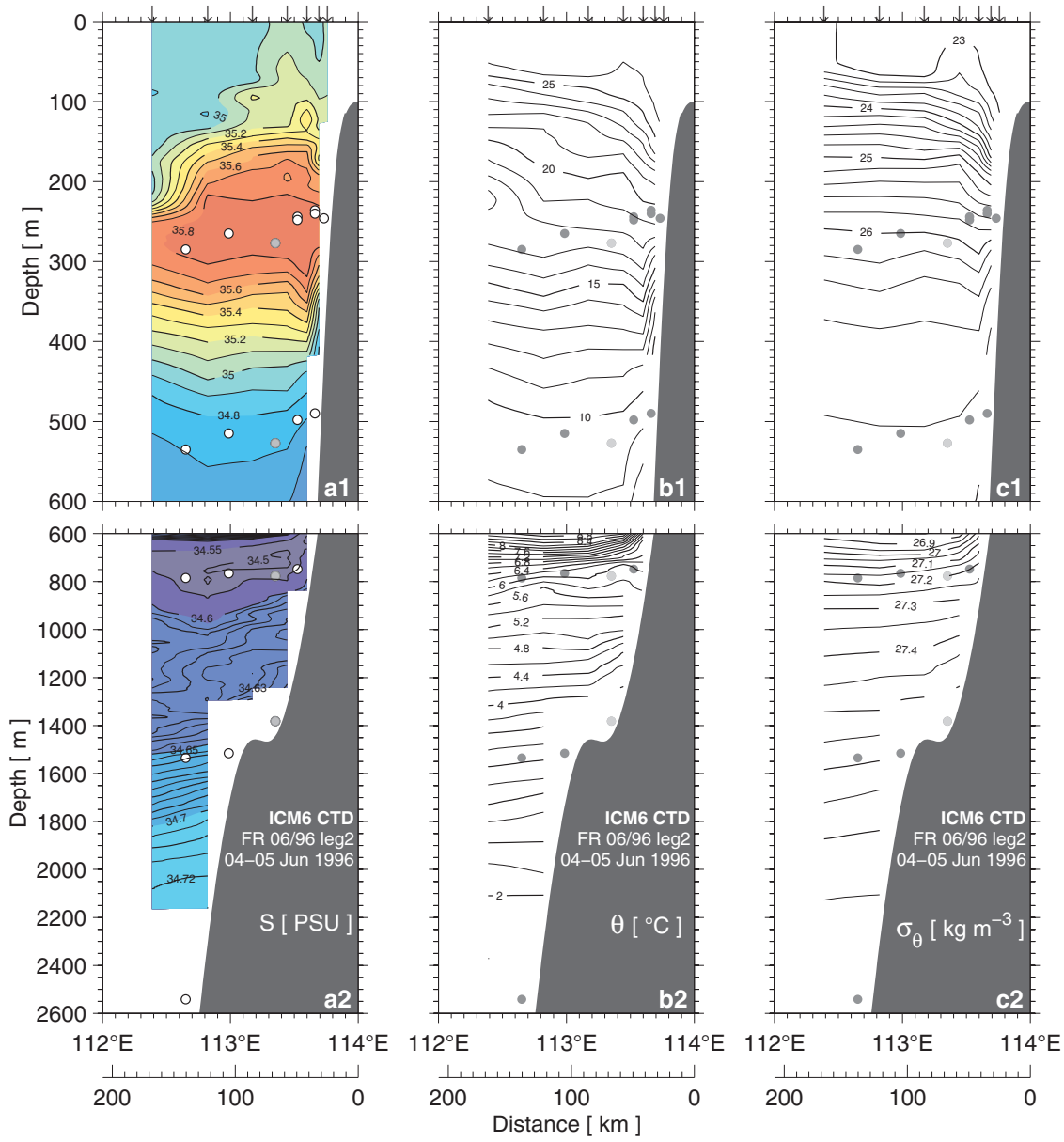

Figure 3.20. ICM6 Hydrographic sections during voyage FR 06/96 leg2. The section is split in upper (1) and deeper (2) ocean. Circles denote current meters, white (recovered) and gray (not recovered). CTD stations are indicated by downward pointing arrows.

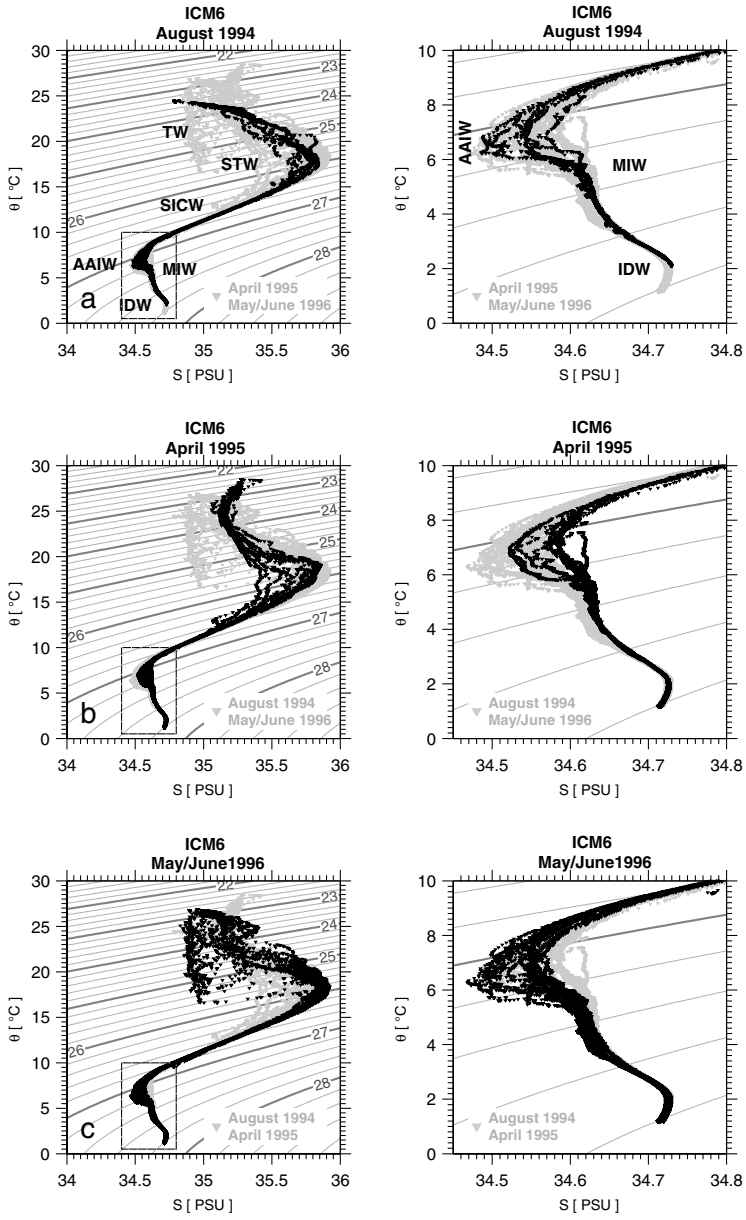

Figure 3.21. ICM6 θ–S diagrams (left) and zoom (right). (a) August 1994; (b) April 1995; and (c) May/June 1996. Black symbols are associated with the title of each diagram (cruise in discussion) while gray symbols are plotted only for reference and are associated with the other ICM6 cruises as indicated in the bottom of each diagram. TW (Tropical Water). STW (Subtropical Water). SICW (South Indian Central Water). AAIW (Antarctic Intermediate Water). MIW (Mixed Intermediate Water). IDW (Indian Deep Water).

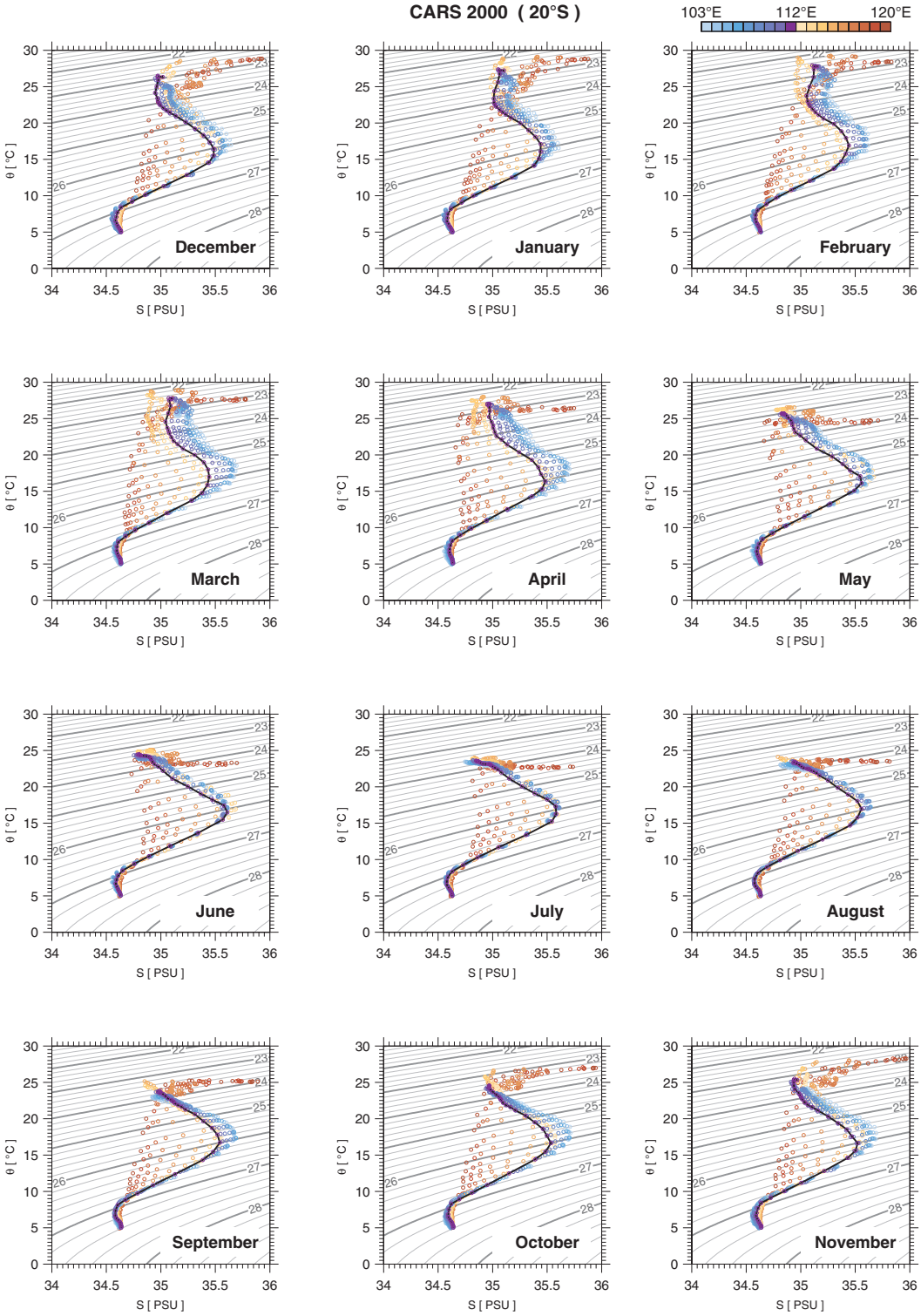

Figure 3.22. CARS seasonal θ–S diagrams at 20°S. Variation in colour of the symbols represent variation of the longitudinal location , from 103° to 120°E, as indicated by the colorbar on the top right. The continuous θ–S line is at 112°E.

3.3.4 Source water inferences

Some inferences about the regional flow patterns are made by comparing θ–S curves from ICM6 with JADE and WOCE. Comparisons are organised by ICM6 cruise periods – August 1994 [**Figure 3.23**], April 1995 [**Figure 3.24**] and May/June 1996 [**Figure 3.25**] – and flow inferences are described according to the water masses identified in **Section 3.3.3**, from surface to intermediate depths. A schematic diagram of the inferred flow patterns is sketched in **Figure 3.28**.

3.3.4.1 Tropical Water

The source area for the TW found at 22°S lies to both northeast (JADE lines) and northwest (WOCE lines) sides of ICM6, and is delimited in the north by a well defined hydrological front in salinity, oxygen and nutrients along 14°–16°S [Fieux *et al.*, 1996; Coatanoan *et al.*, 1999; Wijffels *et al.*, 2002]. More precisely, this area is a tropical–subtropical transition zone between the South Equatorial Current and the southeastern Indian Subtropical Gyre. Although the TW characteristics associated with this zone is not as warm and fresh as Indonesian Surface Water (ISW) [Gordon and Fine, 1996; Wijffels *et al.*, 2002], it may hold an analogous near isohaline distribution over temperature in θ–S space. Perhaps this suggests that some ISW carried to the west by the South Equatorial Current (14°–16°S) retroflects as the Eastern Gyral Current (18°–20°S). The latter eventually diverges part of its eastward flow into a poleward flow that feeds into the Leeuwin Current. Along its path to the subtropics, TW gradually loses heat and gains salt as a result of air–sea transformations and mixing with cooler and more saline STW. These two factors together with changes in the advection patterns of the source area most probably account for the different θ–S relationships seen at 22°S. At some stage, south of 22°S, TW is likely to be completely modified into STW.

The ICM6 θ–S profile from August 1994 is apparently explained by TW coming from both the northeast (JADE) and northwest (WOCE) parts of the source area [**Figure 3.23**]. The characteristics of the water within the warm and fresh surface cap matches the JADE observations [panel a]. Its poleward advection to 22°S most probably happens through Ekman transport, largely favoured by the predominant winds in austral winter [Hellerman and Rosenstein, 1983; Godfrey and Mansbridge, 2000]. In contrast, the characteristics of the water below the surface cap matches the WOCE observations [panel c], suggesting that little of the near isohaline TW in the northeast part of the source area makes its way to 22°S during the winter season. This agrees with observations that point to a northeast surface flow from September to January in that region [Wyrtki, 1962; Cresswell *et al.*, 1993].

The ICM6 θ–S diagram from April 1995 [**Figure 3.24**] seems to be explained by water inflow from the northeast (JADE) part of the source area. Its TW profile depicts two

clear tilts, a very warm and saline surface cap, likely produced by summer heating and evaporation over the North West Shelf, on top of a mixing line that connects the fresher and warmer water with more saline and cooler water. As the WOCE April 1995 [panel c] lies in a location slightly to the west of ICM6 and show signs of a cooler and more saline near surface water than JADE February/March 1992 [panel a], it suggests that the supply of TW to the ICM6 site originates from the northeast part of the source area, corroborating the inferences made in **Section 3.3.2**, in which a positive SLA favours a coastally trapped poleward flow along the Australian coast from 18°S [**Figure 3.13**, panels b1, b2].

The ICM6 θ–S diagram from May/June 1996 [**Figure 3.25**] is an interesting case. Its near isohaline profile of relatively low salinity is closely matched by the θ–S properties from JADE February/March 1992 [panel a] and also from WOCE April 1995 [panel b], indicating a possible inflow to 22°S from both northeast and northwest of ICM6. However, in **Section 3.3.2**, we have inferred that this low salinity is possibly justified by advection of TW from the northeast of ICM6 based on the monthly CARS θ–S diagrams across 20°S [**Figure 3.22**]. The SLA snapshots suggest an onshore flow approaching the ICM6 from west [**Figures 3.12** and **3.13**]. But as SLAs show large temporal variability the inferred flow may not be representative of longer time periods. Thus, it seems that the flow pattern associated with the near isohaline profile of relatively low salinity from May/June 1996 may be better understood through the comparison with CARS, or in other words, water inflow from the northeast of ICM6. With respect to the mixing line that connects fresher and warmer water with more saline and cooler water, which is the other TW profile seen in May/June 1996, its characteristics are likely explained by water inflow from the north–northwest part of the source area, as indicated by the bluish colours in **Figure 3.22**.

3.3.4.2 Subtropical Water and South Indian Central Water

At 22°S, STW and SICW are carried equatorward by the Leeuwin Undercurrent at 200–300 and 400–500 m depth respectively. Some past studies have also shown STW and SICW within the Leeuwin Undercurrent at southern latitudes than ICM6 [e.g., Thompson, 1984; Smith *et al.*, 1991; Toole and Warren, 1993]. Their primary fate is to flow northwestward along the northern edge of the southeast Indian Subtropical Gyre [You and Tomczak, 1993; Wijffels *et al.*, 2002]. This pathway is similarly deduced herein. For instance, the difference in the STW salinity maximum between JADE (35.2 psu) and ICM6 (35.8 psu) [**Figures 3.23** and **3.24**, panel a] seems too large to purely result from mixing, given the short distance between the sites. Therefore a major fraction of STW/SICW must turn northwestward and only a smaller fraction proceeds to the northeast of ICM6, in agreement with earlier work [Fieux *et al.*, 1996; Coatanoan *et al.*, 1999; Wijffels *et al.*, 2002]. Although pathways for STW/SICW have been pointed out before, the question to raise is whether the secondary path implies that the Leeuwin

Undercurrent turns North West Cape to continue north of 22°S, along the North West Shelf area. The JADE observations from August 1989 [**Figure 3.23**, panel a] show a STW salinity maximum near the coast. In February/March 1992 [**Figure 3.24**, panel a], this maximum lies further offshore and a roughly isohaline distribution of lower salinity is found instead in the coastal stations (#1–5). This perhaps implies that if the Leeuwin Undercurrent continues to the North West Shelf, it is not an equatorward year–round flow in that region.

During winter, STW and SICW are subducted at subtropical latitudes of the southeast Indian Ocean (25–35°S and 40–45°S respectively) and transported to the tropics at thermocline depths [You and Tomczak, 1993; Karstensen and Tomczak, 1997; Karstensen and Quadfasel, 2002b]. Particularly in the case of STW, there are two potential source regions with surface salinities of 35.8 psu or higher [**Figure 3.26**], produced by excess of evaporation over precipitation. One source region is centred at 30°S and 105°E, off the west coast of Australia, and the other lies off the southern coast, in the Great Australian Bight. Taking into account that the region off the southern coast is of a more local production and STW has been traced to flow eastward along the South Australian Basin [Bye, 1986; Godfrey *et al.*, 1986; Rochford, 1986; Herzfeld, 1997], the most probable supply of STW to the Leeuwin Undercurrent seems the region off Western Australia.

3.3.4.3 Antarctic Intermediate Water

AAIW is formed in the Antarctic Polar Zone and is advected into the South Indian Ocean at different locations to recirculate within multiple basin gyres [Fine, 1993; Toole and Warren, 1993]. In the Perth Basin, its broad scale pathway is part of the southeastern Indian Subtropical Gyre [You, 1998; Sloyan and Rintoul, 2001]. The water property contrast in the θ–S diagrams suggests the same picture. The AAIW salinity minimum is more attenuated at 22°S than at 24°S [**Figures 3.23** and **3.24**, panel d] and it apparently vanishes along the JADE sections [**Figures 3.23** and **3.24**, panel a]. This implies that AAIW is advected equatorward at 22°S by the deeper part of the Leeuwin Undercurrent, approximately at 500–700 m depth [see mean velocity in **Figure 3.4**], but to the north of this latitude, AAIW is mainly transported westward along the northern limb of the Subtropical Gyre.

3.3.4.4 Mixed Intermediate Water

At intermediate depths, there are three water masses in the Indian Ocean, fresh AAIW (Antarctic), fresh Indonesian Intermediate Water (IIW), and salty North Indian Intermediate Water (NIIW). NIIW originates from highly saline Red Sea and Persian Gulf

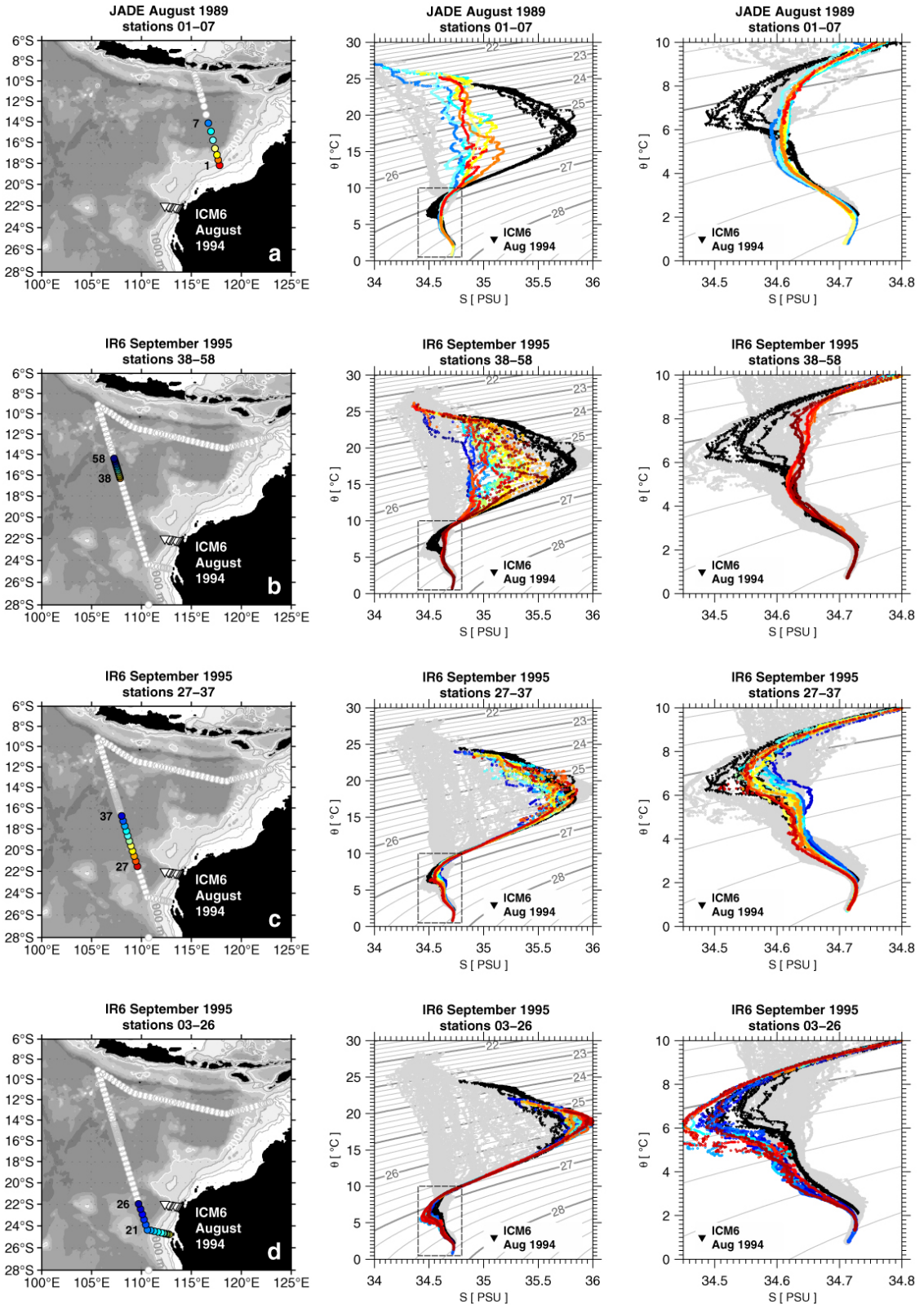

Figure 3.23. August 1994 θ–S diagrams comparisons. Black symbols are ICM6 data while coloured symbols are JADE or WOCE, as indicated and identified by station location (left). Gray symbols are JADE or WOCE observations only used for reference. Right panels are zoom at depth.

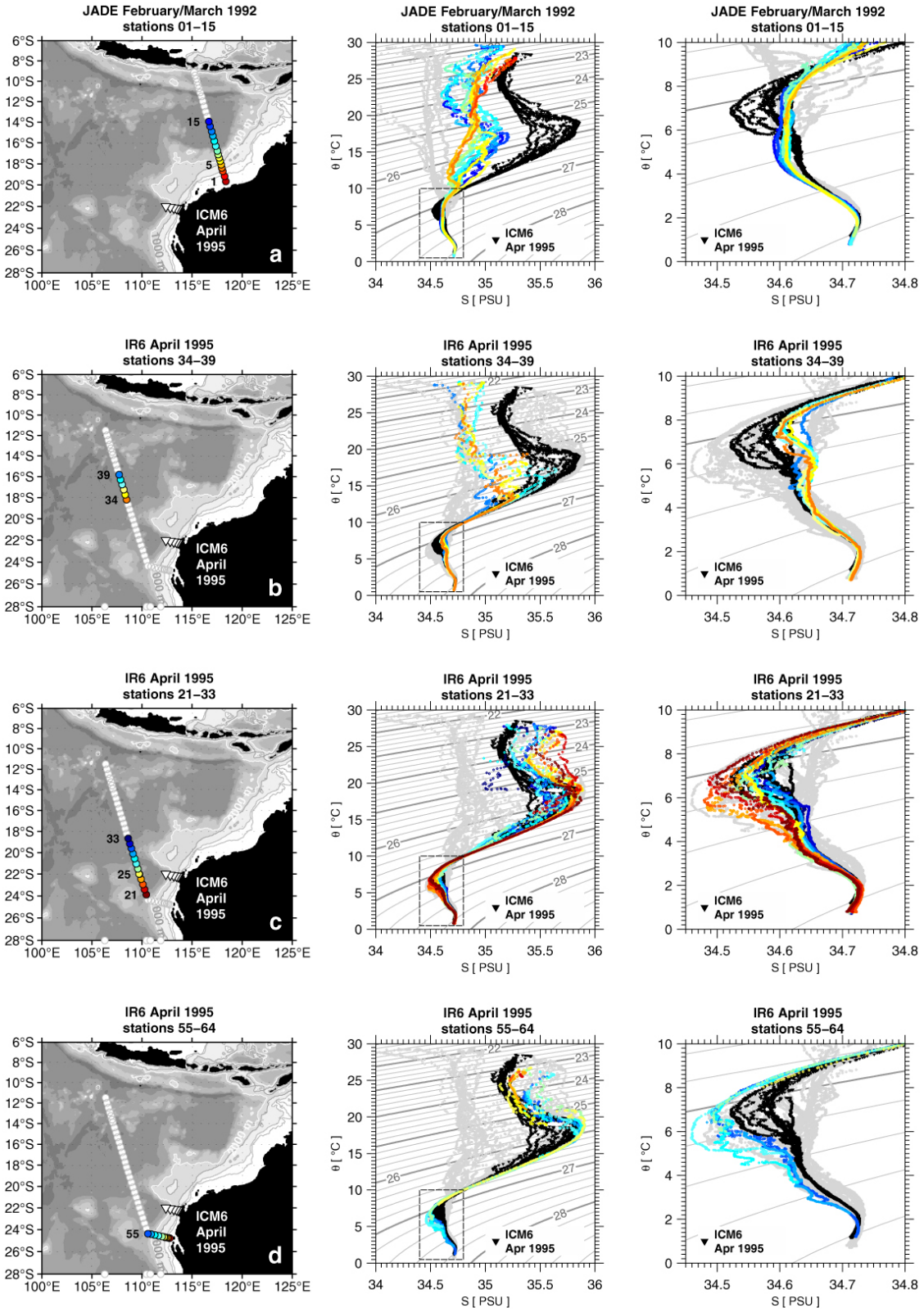

Figure 3.24. April 1995 θ–S diagrams comparisons. Black symbols are ICM6 data while coloured symbols are JADE or WOCE, as indicated and identified by station location (left). Gray symbols are JADE or WOCE observations only used for reference. Right panels are zoom at depth.

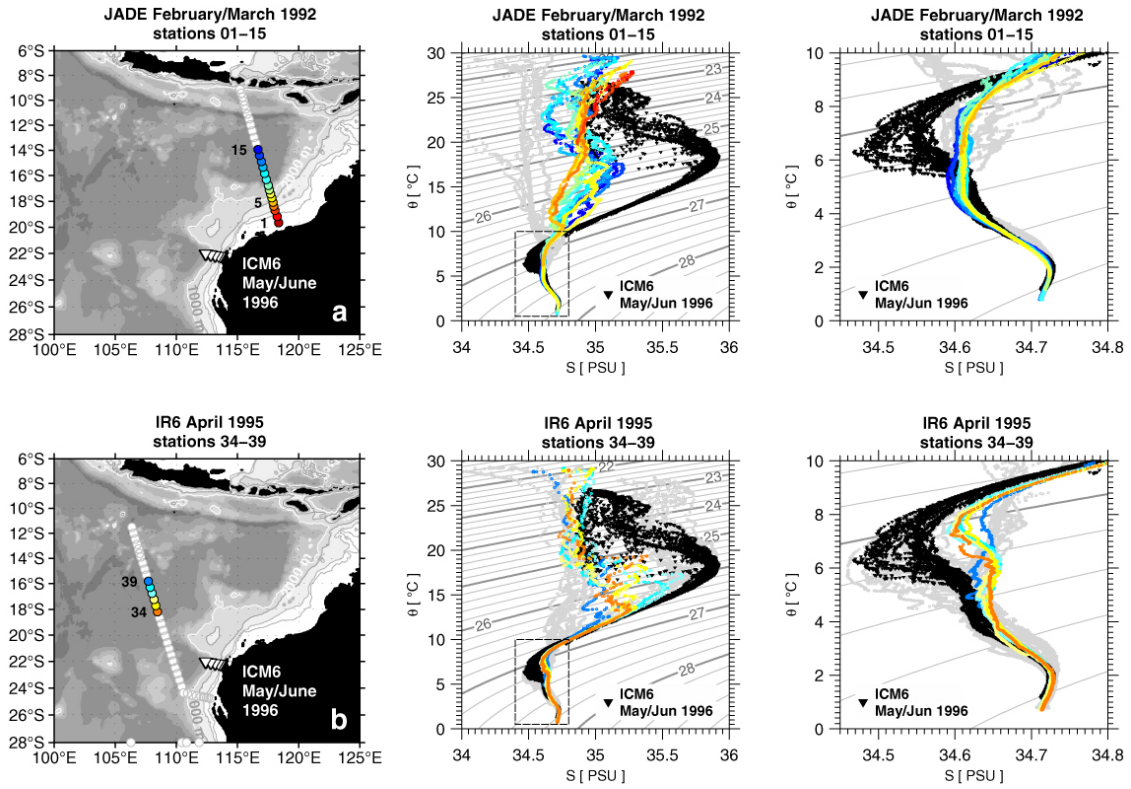

Figure 3.25. May/June θ–S diagrams comparisons. Black symbols are ICM6 data while coloured symbols are JADE or WOCE, as indicated and identified by station location (left). Gray symbols are JADE or WOCE observations only used for reference. Right panels are zoom at depth.

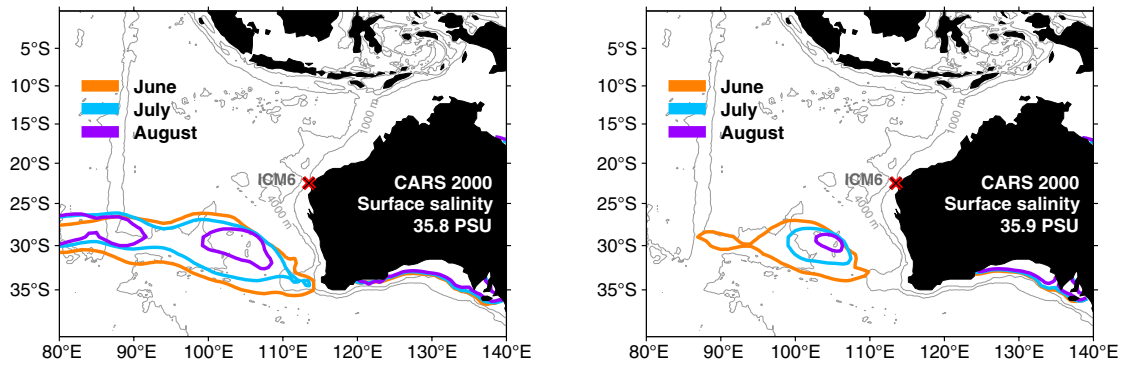

Figure 3.26. CARS sea surface salinity 35.9 (left) and 35.8 (right) psu contours for wintertime in the southeastern Indian Ocean. Isobaths are 1000 and 4000 m. ICM6 current meter location is represented by the red/black cross near 22°S

outflows in the remote northwestern Indian [Rochford, 1961; Rochford, 1964; Rochford, 1966]. Although the overflow is small in volume and mixes with fresher cross–equatorial intermediate water, its saline signal survives long distances. Traces of NIIW in the southeastern Indian Ocean were first suggested by Rochford [1961], as far south as 22°S (100°E), and with less certainty to ~32°S. Maps of potential vorticity gradient in Beal *et al.* [2000] indicate that the spreading of NIIW is primarily zonal between 10°–23°S while a relatively free meridional flow may exist south of 23°S. Wijffels *et al.* [2002] have recently confirmed eastward advection of mixed NIIW at ~16°–18°S, between the westward South Equatorial Current transporting IIW and the northern limb of the Subtropical Gyre carrying AAIW, as revealed by normalised salinity anomaly transects from the same JADE and WOCE observations as analysed in this study.

In this study, MIW refers to a mixing product of AAIW, IIW and NIIW. At 22°S, MIW is found at ~900–1400 m and is depicted by a near isohaline (~32.63 psu) profile within the ~4° to 6°C temperature range. This θ–S relationship, however, varies with location. Northwest of ICM6, MIW is detected by a salinity maximum on the ~27.2 kg m^{-3} [**Figure 3.24**, panel b], the mixed NIIW at ~16°–18°S reported in Wijffels *et al.* [2002]. To the south of ICM6, and north of ~24–26°S, the salinity maximum gradually attenuates [panels c, d]. We may either assume that MIW moves poleward along the coast from a diversion of the eastward flow at ~16–18°S or that multiple narrow eastwards jets (with variable NIIW content) approach the Australian coast as suggested in Beal *et al.* [2000].

A very similar MIW product, with an obvious “salinity signature” from the Red Sea and Persian Gulf, is also advected poleward by the Agulhas Current along the African coast [Beal *et al.*, 2000; Donohue and Firing, 2000; DiMarco *et al.*, 2002]. **Figure 3.27** illustrates how the MIW properties at ~25°S in the Agulhas Current (western boundary) compare to those at 22°S (eastern boundary). Both AAIW and MIW are colder (denser) and have a larger difference between their respective salinity extrema in the western boundary (Mozambique Channel) compared to the eastern boundary (North West Cape).

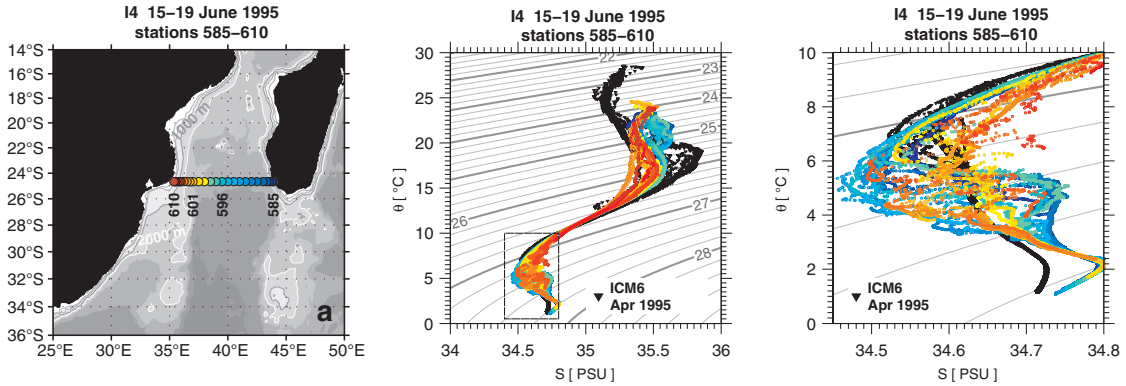

Figure 3.27. θ–S diagram comparison. Black symbols are ICM6 data in the eastern boundary (22°S) while coloured symbols are part of the WOCE I4 line in the western boundary (25°S), as indicated and identified by station location (left). Right panel is zoom at depth.

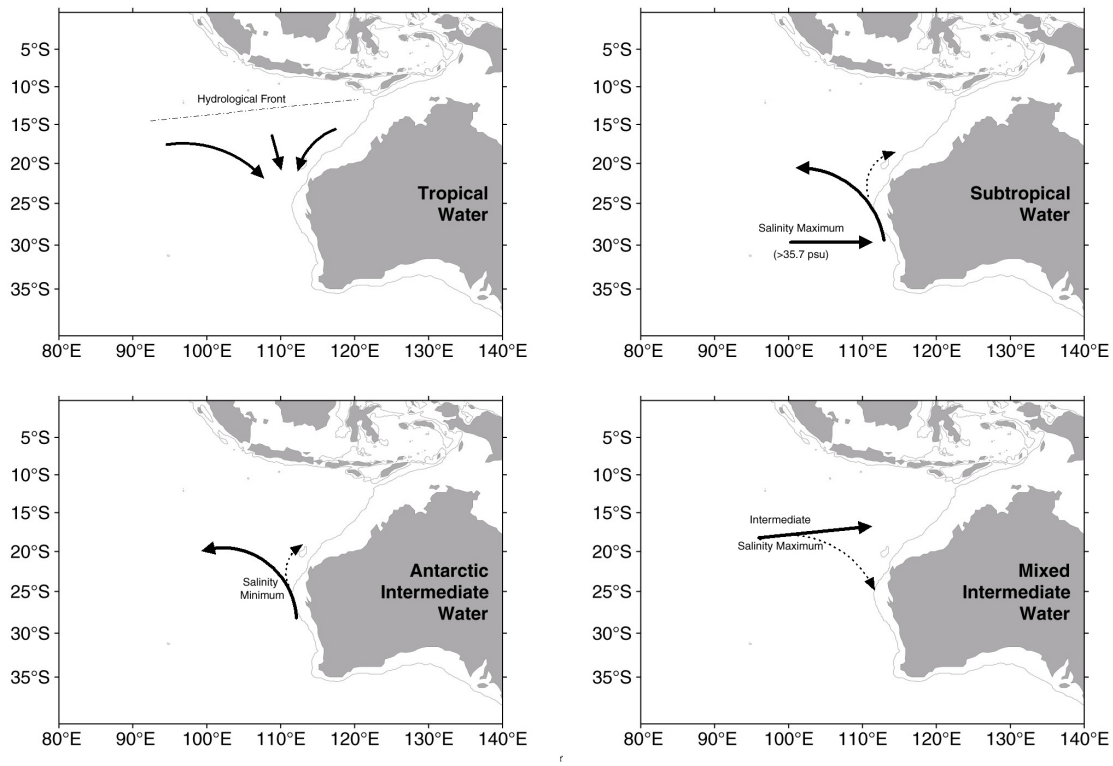

Figure 3.28. Schematic diagram for inferred flow patterns, from surface to intermediate depths.

3.4 SUMMARY AND DISCUSSION

In the nearly two years of the ICM6 direct observations, August 1994 to June 1996, the Leeuwin Current emerges as a coastally trapped poleward jet with a subsurface maximum at ~80 m depth close to the shelf edge, transporting relatively warm and fresh Tropical Water to southern latitudes of the west Australian coast. Maximum speeds range from –6 cm s^{-1} in the 363–day mean to –12 cm s^{-1} in the longest 640–day mean, suggesting a strengthening Leeuwin Current towards the 1996 season, a La Niña year. Its depth reaches about 200 m near the coast but does not penetrate more than 150 m further seaward. Its upper portion lies within the mixed layer while its lower portion intrudes into the seasonal (pycnocline) thermocline. Its width at 22°S remains an open question as measurements in the top 200 m were made only within a narrow portion of the section, ~20–30 km wide, which did not span the shelf nor did it extend further than 50 km distance from the coast (mooring 3). Indirect evidence, however, suggests that the Leeuwin Current is either very wide and/or converges with a branch of the Eastern Gyral Current at ~22°S. Shortcomings in the direct observations appear to account for a rather small volume transport of –0.26 ± 0.02 Sv (640–day mean) with no clear seasonal variability. Significant ageostrophic noise in the synoptic data invalidated the geostrophic estimates obtained from the thermal wind approximation. Changes in the θ–S content of the Tropical Water carried by the Leeuwin Current, as seen in August 1994, April 1995 and May/June 1996, likely arise from seasonal and interannual variability in water mass transformation (driven by air–sea fluxes) and in advection patterns in the source region. Tropical Water is fresher and warmer around May–June, but it is even fresher and warmer during La Niña years. The potential source region for the Leeuwin Current at 22°S comprises a coastally trapped area off the North West Shelf and the adjacent tropical ocean found south of a zonally stretched hydrological front along ~14°–16°S, a transition environment between the tropics and subtropics.

Past studies have argued that the Leeuwin Current tapers, deepens, accelerates and increases volume transport as it moves poleward along the west Australian coast. While meandering of the Leeuwin Current beyond the limits of the ICM6 array, as detected in SST images, along with gaps in the direct observations caused a number of difficulties, we could verify that the Leeuwin Current at 22°S is shallower by about 100 m than at ~30°S. If the lateral extent of the Tropical Water layer in the ICM6 cross–shelf sections is taken as an indicator of the Leeuwin Current at 22°S, the current's width is very broad, at least ~200 km. Otherwise, the "broad Leeuwin" seems to result from a confluence with the Eastern Gyral Current (more likely). This current is reported in the literature to transport Subtropical Water but it is shown herein that both Eastern Gyral and Leeuwin Current should contain relatively warm and fresh Tropical Water, however, not as fresh as the Indonesian Surface Water carried by the South Equatorial Current. Even under constant air–sea transformation the low salinity and warm signal of the

Tropical Water advected poleward by the Leeuwin Current survives vast distances in the subtropics [Cresswell and Golding, 1980; Rochford, 1986; Cresswell and Peterson, 1993]. Tropical flora and fauna are consequently advected to higher latitudes than would otherwise be expected. For instance, there are reports of tropical species of clear Indo Pacific origin along the Australian coastline as far as the region of the Great Australian Bight [Markina, 1976; Maxwell and Cresswell, 1981].

The equatorward Leeuwin Undercurrent is marginally resolved in the ICM6 direct observations but a picture is elaborated with support of the property distributions. At 22°S the undercurrent vertically stretches from 150–200 to 500–750 m depth, with maximum speed at 200–300 m, near the upper slope. The mean maximum velocity of 4 to 6 cm s^{-1} at ~210 m depth captured in the direct observations is only the edge of the true current maximum. At higher latitudes, the Leeuwin Current is deeper so the undercurrent's depth is likely to reach down to 800–900 m. At 29.5°S its maximum mean speed is faster than at 22°S and lies at ~450 m depth [Smith *et al.*, 1991]. Based on synoptic Lowered–ADCP observations from cruise surveys in April and November 1995, Sprintall *et al.* [2002] suggested that the Leeuwin Undercurrent at 25°S has a two core structure centred at ~250 m and ~700 m, being the equatorward flow strongest in November. With ICM6, we could not verify any seasonal pattern or double core structure. The difference in the core magnitude and depth location between ICM6 (~5 cm s^{-1} at ~200 m, 22°S) and LUCIE (~9 cm s^{-1} at ~450 m, 29.5°S) implies that the undercurrent weakens and rises upstream, in agreement with inferences made in past studies.

The Leeuwin Undercurrent advects Subtropical Water (salinity maximum), South Indian Central Water and Antarctic Intermediate Water (salinity minimum) along the west Australian coast to lower latitudes of the Indian Ocean. The primary fate of these water masses is to flow westward along the northern limb of the southeastern Subtropical Gyre. A secondary fraction continues along the coast towards the North West Shelf, but we suspect that the undercurrent is not a permanent flow in that region. Off the west Australian coast, Subtropical Water seems to be advected by both the Leeuwin Undercurrent and Leeuwin Current. Cross–shelf sections in Smith *et al.* [1991] show a salinity maximum at Leeuwin Current depths off Fremantle (32°S) and Cape Mentelle (34°S) while at Leeuwin Undercurrent depths off Shark Bay (25°S) and North West Cape (22°S). Subtropical Water is seen in the undercurrent across the ICM6 section at 22°S, but not in the Leeuwin Current. Following these observations and the fact that the source area for Subtropical Water, with a salinity maximum of 35.8 psu or higher, lies in the ocean surface centred at ~30°S, away from the coastal boundary, we conclude that the eastern boundary of the South Indian Ocean exports salt both equatorward with the Leeuwin Undercurrent (permanent thermocline) and poleward with the Leeuwin Current (seasonal thermocline). Moreover, as the Subtropical Water source region sits in the open ocean, it implies that zonal (and downwelling) flows must approach the coastal boundary to feed into the Leeuwin Undercurrent, and not only into the Leeuwin Current as previously held. These subtropical flows preferentially supply water to the Leeuwin

Current at higher latitudes while to the undercurrent at lower latitudes (where the Leeuwin Current is shallower). So, most possibly south of 30°S, the Leeuwin Undercurrent may only contain South Indian Central Water and Antarctic Intermediate Water, as Subtropical Water is advected poleward within the Leeuwin Current.

In the same manner studies argue that onshore subtropical flows and the Leeuwin Current are driven by an alongshore pressure gradient off Western Australia, the Leeuwin Undercurrent is thought to be driven by a reversed alongshore pressure gradient at depth, caused by a deeper thermocline in the subtropics [Thompson, 1984; Godfrey and Ridgway, 1985; Godfrey and Weaver, 1991]. So, at depths of the Leeuwin Undercurrent, one probably would also expect offshore flows rather than onshore flows. It is most likely that both coexist, however, we still need to understand the physical processes which explain the link between the water masses distribution, the zonal jets (onshore and offshore) and the boundary currents (Leeuwin Current and Leeuwin Undercurrent). If the mechanisms that govern the Leeuwin Current and its undercurrent are strongly coupled, it may explain why a more saline Undercurrent is simultaneously observed along with a fresher Leeuwin Current in La Niña years.

The current patterns below the Leeuwin Undercurrent have not been measured directly before ICM6, and they reveal a richer vertical structure than initially expected. Immediately below the undercurrent there is a mean poleward flow of –0.8 cm s^{-1} (363–day mean) at 785 m depth carrying a mixed Intermediate Water, which saline signs can be traced back to overflows from the Red Sea and Persian Gulf [Wijffels *et al.*, 2002]. At 1535 m the current is equatorward, with a 641–day mean of 0.5 cm s^{-1}. At 2541 m the flow is poleward again, –0.6 cm s^{-1} (641–day mean) and embedded in Indian Deep Water. Narrow and bottom–intensified poleward flows are observed along the continental slope, at 490 m and 1515 m. It is not clear whether the current found at 490 m is a deep extension of the Leeuwin Current or an independent feature. Its velocity mean for the initial 363 days is –2.6 cm s^{-1}, but because of an equatorward reversal, which might be related to a long term weaving of the water column, the value decreases to –0.51 cm s^{-1} in the 471–day mean. At 1515 m, the mean velocity is –2.4 cm s^{-1} (470–day mean). Many direct observational analyses arising from the WOCE effort have also depicted bottom–intensified flows, suggesting that these features are a more common part of the circulation than previously thought [e.g., Yoshikawa *et al.*, 2004].

Statiscally the ICM6 current and temperature time series (12–21 months) are too short to confidently determine the dominant low frequency variabilities, nevertheless some patterns are clearly evident. Higher frequency variability (flow transitions in a couple of days) prevails near the surface and along the slope waveguide, where coastally and bottom–trapped waves propagate. Lower frequency variability (flow transitions in a couple of months), such as mesoscale eddies with a period around 60–180 days, dominate at ~200–800 m depth, away from the boundary. These mesoscale features appear to correspond to the semi–annual Rossby waves detected in altimetry [Morrow

and Birol, 1998]. The ENSO–related warming in the temperature time series penetrates down to 1515 m depth within the coastal waveguide. In contrast, a cool drift is verified in the deepest instrument at 2541 m depth. Considering that the ENSO wave forcing the weaving of the thermocline is largely explained by the first two baroclinic modes [Clarke and Liu, 1994], a reverse in the temperature trend at depth is expected. So there is a chance that the observed cool drift might also be ENSO–related.

3.5 CONCLUSIONS

The picture of the Leeuwin Current and Leeuwin Undercurrent provided by the ICM6 and complementary observations generally shows good correspondence with previous studies but they also reveal new insights of the regional circulation:

- At 22°S the Leeuwin Current is a shallow narrow and subsurface–intensified but relatively weak poleward flow which exclusively carries Tropical Water from north of 22°S. Its temperature and salinity content is variable and set apart by distinct θ–S curves. The θ–S curves are presumably linked with seasonal and interannual variability in water mass transformation driven by air–sea fluxes and in advection patterns of the source areas. The source areas lie just off the North West Shelf and the open ocean along the Eastern Gyral Current domain (16°–18°S), a transition environment between the tropics and subtropics. The Tropical Water carried by the Eastern Gyral Current is not as fresh and warm as Indonesian Surface Water transported by the South Equatorial Current (10°–14°S).

- Past studies inferred that a broad onshore geostrophic flow, driven by alongshore pressure gradient, augment the poleward flow of the Leeuwin Current along the west Australian coast with Subtropical Water (salinity maximum). At 22°S Subtropical Water is carried equatorward by the Leeuwin Undercurrent. The source area for Subtropical Water lies at surface near ~30°S, in the middle of the Subtropical Gyre. An onshore flow must bring this water to the coast to be advected by the Leeuwin Undercurrent and not only by the Leeuwin Current as previously held. Consequently, the eastern boundary of the South Indian Ocean exports salt in both directions, poleward and equatorward, at seasonal and permanent thermocline depths respectively.

- Synoptic and mesoscale variability dominate the nearshore and offshore parts of the array site respectively. Synoptic variability is presumably caused by locally or remotely forced coastally trapped waves. Some of the synoptic fluctuations are clearly associated with the passage of tropical cyclones, which cause temporary peaks in the poleward transport of the Leeuwin Current. Mesoscale variability (60–180 days) is strongest between 200–800 m depth, and is likely explained by the semi–annual Rossby waves first observed in altimetry by Morrow and Birol [1998].

- The equatorward Leeuwin Undercurrent at 22°S carries Subtropical Water (salinity maximum), South Indian Central Water and Antarctic Intermediate Water (salinity minimum) between 150–200 m and 500–750 m depth. Below the undercurrent, a poleward flow spreads a mixed Intermediate Water at ~800–1400 m depth, which partially owes its salinity characteristics to outflows from the Red Sea and Persian Gulf. Compared to the western boundary (Agulhas Current along the African continent at 25°S), in the eastern boundary this mixed Intermediate Water is warmer and fresher and its salinity signal attenuates rapidly poleward. Interleaving between Antarctic Intermediate Water and mixed Intermediate Water is conspicuous in the θ–S diagrams.

- Relatively narrow and bottom–intensified currents, directly observed for the first time, are prominent features of the current regime at 22°S.

- The ENSO signal, characterised by a warmer and deeper thermocline during La Niña years, penetrates down to at least ~1500 m within the coastal waveguide at 22°S, and possibly has a reversed sign at ~ 2541 m depth.

In the next chapter, we follow water parcels to determine the pathways and source areas in the tropical and subtropical Indian Ocean linked with the boundary flows and water properties of the Leeuwin Current and Leeuwin Undercurrent along the west Australian coast by means of an online Lagrangian numerical particle tracking.